UNIVERSITY OF CRETE
Department of Physics

Neutrino radio signatures with Argos

Master Thesis

submitted in partial fulfillment of the requirements
for the degree of

Master of Science in Advanced Physics

Emmanouil Foukarakis
under the supervision of Prof. Pavlidou Vasiliki

Heraklion, September 2023

Contents

Chapter 1

Introduction

One of the most important fields of modern physics is high-energy particle physics. Among the most fundamental pieces of this field are the ultra high energy (UHE) cosmic rays and neutrinos to which this thesis is dedicated to. Many aspects of these particles such as their origin, their production mechanisms and a sensible explanation of all the features that appear in their observed spectrum, remain currently unknown despite the remarkable efforts of scientists to narrow down the possible answers.

Intense astrophysical environments such as supernova remnants (SNRs), active galactic nuclei (AGNs), radio galaxies, pulsars etc, are closely interrelated with the emission of ultra high energy cosmic rays (UHECRs). Scientists in order to fill in the gaps in the understanding of these environments have to interpret information about them by deciphering their unique language written in the form of UHE cosmic rays and their products, cosmogenic neutrinos. Intense debate has erupted among the scientific community with a multitude of theories and different explanations on the table to find a satisfying answer for these UHECR sources.

All the above reasons could not be a better prompt to delve into these prominent particles.

Cosmic rays are high energy particles that move through space having velocities that approximate the speed of light. A remarkable progress has been made for the determination of the origin and the physical mechanisms behind the production of the detected UHECRs. The two currently dominated theories suggest that CRs owe their origin either to astrophysical sources providing acceleration mechanisms capable of accelerating them to energies up to $10^{20}eV$ ("bottom-up" scenario) or as some of the present data and recent reports also suggest to the decay of hypothetical so called "supermassive metastable " particles that are no more than relics of the early universe (top-down or non-acceleration scenario).

The highest energetic cosmic rays are the main source of the under-study UHE neutrinos or otherwise called "cosmogenic neutrinos". Interactions of UHECRs with the universal photon background during propagation from their source to Earth constitute the physical mechanism behind the production of cosmogenic neutrinos. The most dominant CR interaction process is the photo-pion production to the cosmic microwave background (CMB) photons. Generally cosmogenic neutrinos are produced via two principal channels: by pion decay or by neutron decay with the latter particles, called "secondary particles", being parts of the particle "shower" produced during CR-background interactions. These high probability interactions or otherwise known as GZK effect are the main reason of observing a cut-off in the CR spectrum below the energy value of $10^{20}eV$.

Several scenarios regarding the injected composition and the expected injected spectrum of CRs do currently exist and are deeply investigated by simulated propagation models. Depending on which of these scenarios each study model takes into account, different results about the spectrum of CR-produced neutrinos and many of their intrinsic properties, such as the maximum possible energy of a detected event or their flux at low and high frequencies, emerge. The flux of secondary neutrinos, being extremely sensitive to the chemical composition of the sources, can constitute a powerful tool to solve the mystery behind UHECR observations and the most characteristic features of their spectrum ("ankle", "knee").

The question that will inevitably have arisen in any attentive reader is what makes neutrino so special to choose them for intensive study in comparison with the entire chaotic potential spectrum of observable particles. To understand this choice more deeply it is enough to realize that in order to penetrate into the inner workings of the astrophysical objects and to obtain a description of the Universe over a larger range of energies, we need a probe that owes specific characteristics. First of all this probe should be electrically neutral meaning not to interact through electromagnetic forces thus keeping its trajectory unchanged from possible deviations coming from magnetic field presence. Furthermore it must be a stable particle (unstable particles are excluded) capable of reaching us after its long journey from distant sources, and weakly interacting so that it will not be absorbed by matter as photons do. In contrast it should be capable of penetrating regions opaque to photons.

The only candidate currently known to exist with such characteristics is the neutrino. Being nearly massless, neutrinos can travel approximately at the speed of light from the edge of our universe. Since they are not deflected by magnetic fields or absorbed by matter, neutrinos will travel in straight lines till reach us. Thus any detected neutrino since having "memory" of its initial direction, pointing back to its source as being unbent from magnetic

presence, and preserving its energy during its journey, can uncover its source origin unveiling its hidden nature. These properties make them excellent messengers of information about the astrophysical objects or events in which they originate from. Another important factor in our successful choice is that other than photons, neutrinos are the most common particles in the universe with their presence being anywhere. However the neutrinos' "Achilles heel" is their low interaction probability with matter and consequently with our particle detectors, which implies huge demands on the volume of Earth based detectors or techniques of remote coverage of large surfaces to capture a few events.

Neutrino detection can achieved using several techniques such as those using particle detectors, like water Cherenkov tanks or underground drilled photomultipliers in the Antarctic ice, or those that trap neutrino presence through their radio emission. A technique that has received a lot of spotlight on it in recent decades is lunar observations. This method of detection is based on the detection of radio coherent pulses from Earth based telescopes such as the under design and potential construction Argos telescope. These radio pulses are generated through an effect attributed to Askaryan,which was the first to introduce it back in 1962, suggesting that when UHE neutrinos interact with the outer layer of the Moon's surface, called the regolith, they produce radio pulses of extremely short duration. This promising technique already competes with pre-existing ones and being sensitive to ultra high energy neutrinos (over the GZK cut-off energy) can act as a catalyst to confirm the established limits for the maximum energetically possible recording of an event. Moreover the lunar radio technique can highlight or confirm ambitious recent models about neutrino production from "exotic" sources in even higher energies.

The detection of cosmogenic neutrinos acts as a hint about where to direct our telescopes in our search for the origin of the ultra high energetic cosmic rays which in turn unlock the most violent and interesting astrophysical phenomena behind their production.

Chapter 2

Production of UHE cosmic rays

Cosmic rays contrary to what their name suggest, are not actually electromagnetic radiation but were named as such by Robert Millikan in 1926 since scientists at that time believed that they were high energy photons (rays) coming from space (cosmic). It was only later that their true nature was unveiled, that is, they are high energy particles moving through space with velocities approaching the speed of light. Cosmic rays can actually be anything from atomic nuclei that have been stripped out of their atoms, (including the heaviest ones) and thus being charged, to particles like neutrinos, called "astrophysical" to distinguish them from cosmogenic neutrinos produced by UHECR interactions during propagation, electrons-positrons or neutrons with the latter two types to be much less abundant. Cosmic ray photons being mass-less are separated from the bulk of cosmic rays having intrinsic mass and are referred to by their own distinct name such as gamma rays or X-rays.

Victor Hess was the first to discover cosmic rays back in 1912 by conducting balloon experiments with its personal participation in the Earth's atmosphere. His study was focused on measuring the ionization rate of the atmosphere as a function of its altitude. Analyzing the results of his study, that particles with high ability to penetrate space (unlike photons) enter the Earth's atmosphere from above causing its ionization, he verified the existence of cosmic rays.

2.1 Theories of origin

The origin of UHECRs is enshrouded in mystery. The theories about their origin fall into two opposing categories. On the one hand, there exist conventional theories suggesting that charged cosmic ray particles to achieve the

required high energies observed, up to $10^{21}eV$, have to be accelerated to them through specific mechanisms in suitable astrophysical environments such as supernova remnants (SNRs), active galactic nuclei (AGNs), radio galaxies or rotating neutron stars. These theories constitute the so called "bottom-up" scenario.

Alternatively, there are scenarios that do not require acceleration mechanisms or connection to specific astrophysical objects for the CRs to reach these high energies but instead rely on their production from the decay of super-massive meta-stable particles denoted as X (to declare our ignorance of them) originating from physical processes at the beginning of the universe. These processes are under intensive theoretical investigation, deeply preoccupying scientists. The scenario is often referred to as "top-down" scenario or as "non acceleration "scenario for the obvious reasons.

Acceleration of charged particles can be achieved in two ways. The presence of a powerful electric field $\vec{E}$, created in astrophysical regions where a pulsar (rotating neutron star) or a rotating accretion disk threaded by magnetic fields is present, is capable of accelerating directly charged particles to extremely high energies (direct acceleration). This kind of acceleration mechanism is not widely favored due to the difficulty in reproducing naturally the characteristic power-law of the observed CR spectrum which is discussed thoroughly in a later section.

The other way of acceleration, which currently represents the standard theory of CR acceleration, is based on statistical acceleration due to repeated scatterings or "encounters" of the charged particles at shocks, with the latter being ubiquitous in astrophysical situations. This kind of acceleration is known as "Diffuse Shock Acceleration Mechanism" based on Fermi acceleration of the first order. A CR particle after an encounter with a shock, which counts as a crossing an a re-crossing from the shock after the reversal of the particle's path by the magnetic field, gains on average energy proportional to the ratio $\frac{u}{c}$, where u represents the relative velocity of the shock front in terms of the isotropic CR frame, hence the reference as first order acceleration. Shocks are present everywhere in interplanetary space such as in supernovae, supernova remnants expanding in the interstellar medium, in AGNs and in terms of cosmological distances in radio galaxies.

A scenario, however, is also likely to be connected to some gaps in the attempt to match theory and observations. As for the acceleration scenario, it is hardly possible in some astrophysical sources to achieve acceleration of particles up to energies of $100EeV$ corresponding to the highest CR energy observed. And even if it succeeded, a subsequent question arises: how will the particles manage to escape these dense regions of great interaction probability while maintaining their energy. The most favorable sources in

terms of energetics are the radio galaxies. The main problem encountered in this speculation is a matter of distance. Since radio galaxies lie at large cosmological distances greater than $100Mpc$ and provided that CRs are conventional particles such as nucleons or heavier nuclei having energies close to the Greizen-Zatsepin-Kuzmin limit around $10^{19,6}eV$, then due to small mean free path of the order of a few Mpc for photo-pion production regarding nucleons or for photodisintegration processes regarding heavier nuclei, CRs will lose a large fraction of their energy. Thus to explain the high energy end of the CR spectrum through acceleration scenarios, a restriction on the source distance to distances smaller than $100Mpc$ is inevitable. Since the approximate values of the Earth's distance from our galactic center and our galactic edge are $8,2 \cdot 10^{-3}Mpc$ and $0,3Mpc$ respectively, there is a possible place in the theory for CRs of both galactic and extragalactic origin.

Regarding the "top-down" scenario, X particles can originate either from topological defects being formed due to symmetry-breaking transitions in the early universe or can be relics of the early universe, that is, sufficiently massive meta-stable particles that decay in the current epoch. It is clear that X particle decay implies that the X particles have a lifetime comparable to the lifetime of the universe. X particles could constitute dark matter which is material that we can't see and we barely understand but makes up 23% of the universe. The topological defects (TDs) include phenomena such as magnetic monopoles, cosmic strings, domain walls etc. TDs survive indefinitely unless they are physically destroyed through collapse or annihilation releasing energy in the form of massive quanta denoted as X particles of the various fields that constitute the TDs. After the decay of X particles into quarks, gluons, leptons etc., the produced particles form matter, the cosmic ray particles, such as nucleons, gamma rays and neutrinos with energies of the order of the X particles' energies without the use of any acceleration mechanism. The energies of the X particles can far exceed the value of $10^{20}eV$ meaning that CRs with energies much higher than the maximum observed value from accelerating sources can be observed. In models, X particles or TDs may be clustered in galactic halos which implies that if the theory holds, then the dominant contribution in Earth would be from X particles within the Milky Way halo.

No matter how appealing this "top-down" scenario seems with the prospect of opening a path to new fundamental physics and new ideas of the early universe, it is associated with many cons. The most notable of which are that is highly model dependent and it involves as yet untested physics associated with Grand Unified Theories (GUTs) beyond the standard model. Therefore all the scenarios are being tested by the observational flux limits.

Finally, for the determination of the CR origin the mass composition mea-

surements constitute an important factor. Depending on these measurements CRs can either have a Galactic or an Extragalactic origin. Composition measurements confirming protons and light nuclei as the main components of CRs, act as an indication of the presence of extragalactic astrophysical accelerators while measurements confirming heavier nuclei as the main component, act as an indication of galactic CR origin. Last, photon primaries measurements indicate the possibility of 'top-down" scenarios.

Although the general aspects of the CR origin are well identified, significant gaps and uncertainties in reasoning remain. The level of uncertainty is proportional to the CR energy since at higher energies the flux of cosmic rays is drastically reduced. The development and optimization of CR detection methods for the next generation experiments can significantly contribute to deepen their understanding.

2.2 Detection techniques

Reference to CRs is usually restricted to charged nuclei only. This is somewhat justified as electrons, positrons and neutrons are much less abundant achieving a maximum detected energy of a few TeV and the neutral component of γ–ray corresponds to fluxes orders of magnitude lower than the charged CR components of protons and heavier nuclei. Extremely high energy CRs (EHECRs) corresponding to energies of $E \geq 10^{20}eV$ are hardly deflected by magnetic fields since the degree of deflection of CR particles is inversely proportional to the energy. Therefore a potential detection of an EHECR can be linked to its possible source as its arrival direction should point back to it. On the other hand high energetic CR interactions with the photon backgrounds are mainly considered to happen close to their source due to their small mean free path. Thus the CR-produced secondary particles such as neutrinos, when detected on Earth, also having the property of non magnetic deflection, can point back to the CR source. These properties offer us the opportunity of charged particle astronomy and neutrino astronomy to unveil the secrets behind the CR sources.

Cosmic ray primaries of extremely high energy capable of reaching Earth are shielded by the Earth's atmosphere. This implies that direct observations of CRs can only be conducted from space through flying detectors as balloons or spacecrafts. The atmosphere acts as a calorimeter and thus from the initial CR primary interactions secondary particles such as neutrinos, muons and photons are produced. These secondary particles commonly referred to as "air-showers" can then be detected by ground arrays and depending on their properties, the reconstruction of the CR primary can be carried out.

Shower particles are spread over many kilometers until they reach the ground. An interferometer array can thus allow the detection of shower components corresponding to the same initial CR primary. Therefore the measurement of the total number of particles detected can be used to estimate the number of particles in the air shower. Depending on the type of detected particles and the energy model with which are associated, the reconstruction of the energy of the CR primary can be carried out. Furthermore in terms of the CR arrival direction, the measurement of the arrival time difference of the shower particles between different arrays can be used to reconstruct it.

Air shower development is slightly dependent of the type of the primary particle but this dependence is proved to be crucial for the determination of the composition of the CR primaries. If the CR primaries are photons, electrons or positrons which as mentioned above have not been detected at extremely high energies (EHE), then the produced air showers would be muon-poor due to direct electromagnetic cascade development. Thus detecting muon-poor air showers inevitably would mean the existence of such primary particles, consisting an unlikely scenario. On the other hand, if CR primaries are heavy nuclei, then the shower development will occur earlier in the atmosphere, as heavy nuclei are linked with interactions cross sections proportional to the number of nucleons, and faster with fewer generations of secondary particles. Therefore the atmospheric depth, X_{max} measured in $\frac{gr}{cm^2}$, where the number of particles in the shower reaches a maximum, known as shower maximum, is higher up in the air. Another distinction of CR heavier nuclei primaries is that their produced muon content is higher than the one corresponding to light nuclei having started the shower development with the same energy E. Consequently, in order to succeed in determining the composition of the primary rays, knowledge of the X_{max} and muon-content is inevitable.

The detailed development of an air-shower is depicted in the following Figure 2.1 where also detection techniques are present. When CR primaries interact for the first time in the Earth's atmosphere, secondary particles such as pions of all kinds (π^0, π^+, π^-) and other mesons are produced. Being unstable $\pi^0, \pi^\pm$ pions will inevitably decay, the former, into γ–ray photons and, the latter, into muon and neutrinos ($\pi^\pm + \gamma \rightarrow \mu^\pm + \nu_\mu + (\overline{\nu_\mu})$). Gamma ray photons via pair production (see left side of the cascade) produce electron-positron pairs which in turn continue the electromagnetic cascade development via the production of more photons. The production of the latter can be achieved by Bremsstrahlung radiation, which comes from deceleration of an electron due to an attractive force from an ion and a subsequent curve on its trajectory, by Inverse Compton effect, which is associated with relativistically moving electrons interacting with photons and increase their energy

by a factor of γ^2 and finally from annihilation of positrons with electrons of air atoms. The aforementioned descriptions for the production of photons are depicted clearly in the central region of the electromagnetic cascade in the figure.

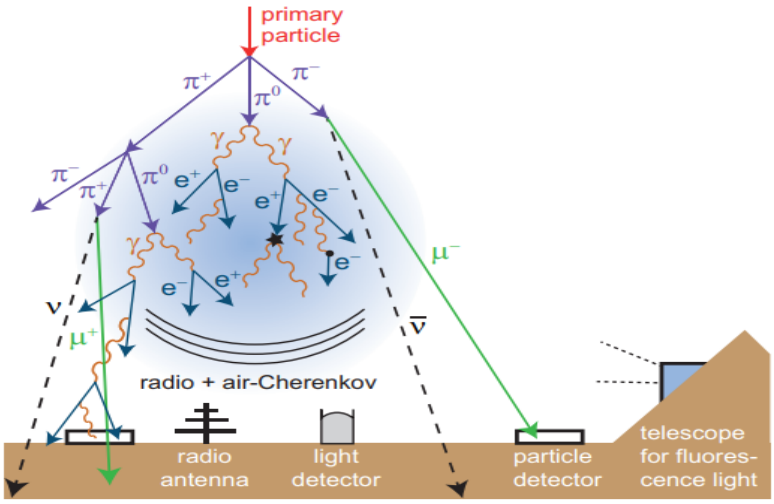

Figure 2.1: Simplistic picture of air-shower development and possible detection tecniques.

The ionization of some air atoms (mostly nitrogen) from incident photons with the apparent extraction of electrons and their inclusion to the shower development, results in the particle cascade developing an overall negative charge excess. The development of the cascade does not continue indefinitely but stops after millions to billions of stochastic interaction processes exhausting the fuel energy of the CR primary. The higher the energy of the CR primary is, the larger the atmospheric depth of the shower maximum. As seen in the figure muons and neutrinos since they are produced, they do not contribute into further shower development but instead can be detected by ground based arrays with a variety of techniques.

The cosmic rays detection techniques can be divided in two categories. The first category includes the direct detection of CR-produced particles either during propagation in space such as cosmogenic neutrinos or when a primary cosmic ray hits the Earth's atmosphere resulting in air-shower particles development, such as muons, electrons and neutrinos. Cosmogenic neutrinos can be detected by ground or underground Earth based particle detectors like enormous water Cherenkov tanks or using physical volumes like the sea water and the Antarctic ice. Examples of experiments based on these techniques

are the High Altitude Water Cherenkov experiment (HAWC) and Super-Kamiokande for water Cherenkov technique, ANTARES and NESTOR in the Mediterranean Sea for sea water experiments and ICECUBE for ice neutrino experiments. To obtain information about the electron-muon ratio particle detectors consisted of different absorbers for each type are used within water Cherenkov or scintillation experiments described below. Last, as already mentioned, the direct observations of CRs can only be achieved by flying balloons or spacecrafts above the Earth's atmosphere.

The second category refers to detection of electromagnetic radiation produced by air-showers directly (air-Cherenkov) or indirectly (air fluorescence, scintillation). Air fluorescence technique refers to the detection of light produced when the secondary particles of an extensive air shower interact with atmospheric atoms and cause its ionization and excitation. Interactions between charged shower particles and nitrogen (N) atoms are the most common ones. A fraction of the gained excitation energy is returned as UV and visible light. The major advantage of this technique is that with a single telescope large atmospheric volumes can be observed. Currently air-fluorescence offers measurements of high accuracy in terms of energy and the position of the shower maximum.

Air-Cherenkov technique detects light produced when charged shower particles like electrons and positrons are moving with speeds exceeding the speed of light in the atmosphere. The light is emitted in the form of a narrow cone moving forward around the particle's radiation. The geometry of the Cherenkov light is justified due to the greater speed of the moving particle with respect to the speed of wave propagation. An overlapping of the produced waves results in the cone form of the emitted light. A scheme depicting the Cherenkov geometry can be seen in Figure 2.2.

Air Cherenkov light is detected at optical and UV frequencies by ground based arrays consisted of photo-multipliers like Tunka-Grande or from imaging telescopes. High accuracy shower-energy measurements are achieved due to the property of radiation of Cherenkov light to scale linearly with the shower energy.

An indirect way of detecting radiation from air-showers is through scintillation detectors. When shower particles as muons or electrons hit a material in a scintillation detector, then the material gets excited and as it deexcites, it reemits radiation, that is it exhibits scintillation. The use of different absorbers for each type of incident particle is the strategy to distinguish muons from electrons. Based on the property of faster electron absorption in comparison with muons, a scintillation particle detector via signal's analysis can estimate the position of the shower maximum. However radiation techniques's accuracy in the measurement of the position shower maximum and

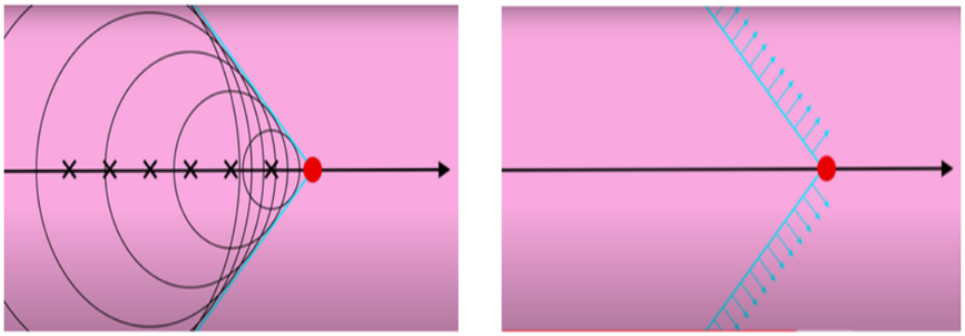

Figure 2.2: Schematic explanation of the cone form of the Cherenkov light.The x's correspond to successive positions of the moving particle. Light isn't emitted just at these locations where the x's are marked but in every point of the particle axis.

consequently in distinguishing the type of the CR primaries remains greater than that of particle detectors.

Radio emission by particle cascades in the atmosphere is produced via two principal mechanisms contrary to the one that exist from particle cascades in dense media like the rock of the lunar regolith. Geomagnetic deflection of charged shower particles such as electrons and positrons leads to electromagnetic emission in the radio part of the spectrum. This kind of radiation can also be achieved due to variation of the charge excess in the shower front caused by CR-primaries interactions with the atmosphere between ranging $20 - 30\%$. For the radio emission in dense media as discussed in section 4.1 the geomagnetic effect is considered negligible. The radiation observed is of the orders of meters in wavelengths, is beamed forward and is mostly coherent. For radio emission of air-showers to be measurable, the radio frequencies should exceed 50GHz which is considered as a high detection threshold. A great advantage of the method though is that is feasible around the clock, meaning during night-hours and bad weather. Examples of experiments using the radio technique for the investigation of high energy CRs are LOFAR and CODALEMA.

A promising technique of radio detection which is associated with cosmogenic neutrinos is based on lunar radio detection by terrestrial ground arrays when UHE neutrinos interact with the outer layer of the lunar surface. As a result narrow radio pulses of nanosecond duration are produced. This case of neutrino detection is discussed in detail in section 4.2.

Combining particle detectors and radio detection techniques described

above and thus forming a hybrid detector like the one used by Pierre Auger Observatory can optimize the chances of achieving higher accuracy in the measurements of the most basic properties of the under-study EHECRs and their shower components.

2.3 Flux spectrum

To get a taste and quickly penetrate into the understanding of the characteristics of the CR spectrum, it would be useful to consider the compilation spectrum of all types of CR particles taking into account the whole range of energies in which they have been observed. Such a compilation spectrum is shown in Figure 2.3.

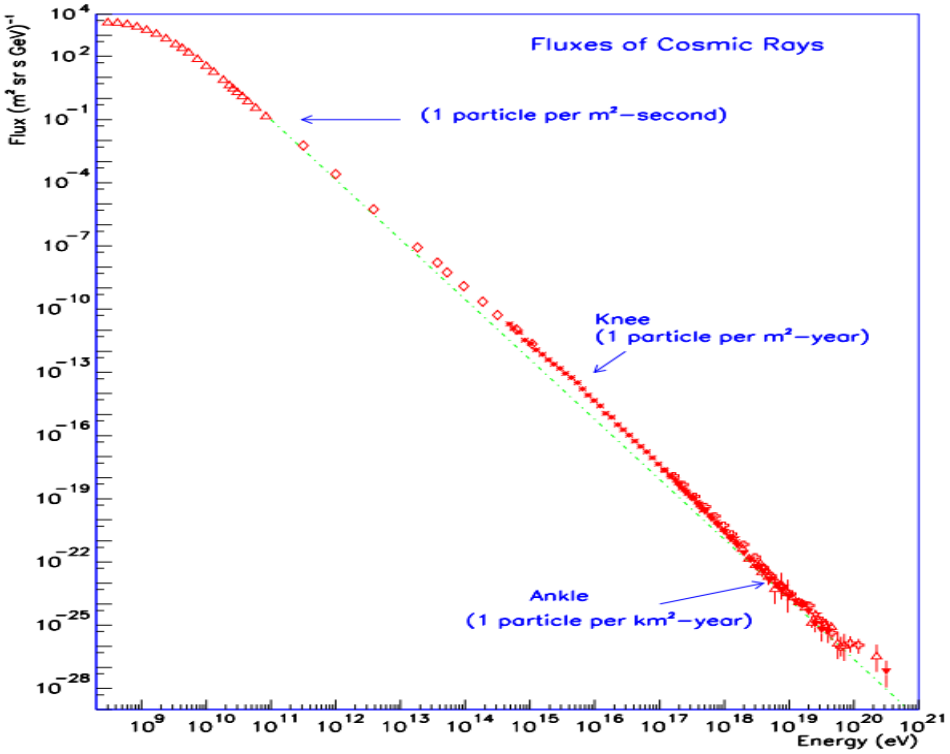

Figure 2.3: Compilation flux spectrum of all types of detected CR particles as a function of the whole detected energy range. The unique features of the "knee" and the "ankle" are also depicted.

The energy range of the spectrum varies from $10^9 eV$ up to $10^{21} eV$, between twelve orders of magnitude in total, and in terms of flux between 32 orders of magnitude. The low flux of high energy CRs is reflected in the low

ratio of particles per unit area per unit time which is inversely proportional to energy. For energies around $10^{9-11}eV$ the CR flux corresponds to 1 particle per m^2 per s whereas for ultra high energies (UHE) around $10^{15-16}eV$ the detection rate decreases to 1 particle per m^2 per year. This region due to the hardening of the spectrum is called the "knee' region. By hardening of the spectrum is meant that its slope changes so that there are relatively more high energy particles. From this point on, the CR observations run out of statistics. That means that direct measurements of CRs cease to be the preferred technique at such high energies. Instead, CR observations are performed via indirect methods meaning the detection of their electromagnetic radiation with various techniques described in the previous section.

Regarding even higher energetic CRs around the values of $10^{18-19}eV$ the flux decreases to so low levels that to make it possible to detect a sufficient number of CRs, the use of giant detectors or the ability to monitor remotely a large volume of a naturally occurring detection medium such as the Antarctic ice or the Moon's surface is required. An example of remotely monitoring of such a naturally detection area has been achieved through the ANITA (Antarctic Impulsive Transient Antenna) experiment aiming to detect radio pulses generated from the CR and neutrino interactions with the Antarctic sheet ice. This high energy part of the spectrum is known as the "ankle". The UHECR flux is so low that even the Pierre Auger detector, whose 1660 water detector tanks contain 12.000 liters of water each, registered only 27 CR events exceeding the energy of $10^{19}eV$ for a time interval between 2004 and 2007 with current detections to be about 30 CR events per year.

The highest CR event ever detected was back in 1991 by the Fly's Eye experiment in Utah desert with the value of its energy being calculated at $(3,2 \pm 0,9) \cdot 10^{20}eV$. The concern, reflection and admiration created by this detectable event of six times higher than the theory allowed were the causes that led to it being named as the "Oh-My-God particle". A couple of years later in 1993 the Akeno Giant Air shower Array (AGASA) recorded an air-shower event of the order of $2 \cdot 10^{20}eV$ being the second highest CR event ever observed. The beginning of the detection of such high energy CR events is associated with the distant 1962 and John Linsley who confirmed the detection of a CR event above $10^{20}eV$ by the Volcano Ranch experiment in New Mexico.

It is clear from previous discussion that the CR spectrum exhibits a power-law spectrum ($\sim E^{-\beta}$) with a steep spectral index β. The power law exhibits significant deviations ("breaks") around the "knee" region, which differ as far as the exact CR energy is concerned based on the composition model, and into a lesser extend to the "ankle". Observational data state that just below the energy of $10^{20}eV$ there is a abrupt dip in the slope of

the diagram. More specifically present data confirm that there is a CR flux cut-off at exactly the energy of $10^{19,6}eV$. Since 1966 the most satisfactory explanation of this feature has been given by Greisen, Zatsepin and Kuzmin ([5]). They stated that the steepening in the spectrum is deeply related with interactions of charged CRs (the dominant component in UHE) during propagation, including both protons and heavier nuclei, to the photon backgrounds (described in detail in chapter 3). The photon backgrounds can either be the 2,7K Cosmic Microwave Background (CMB) radiation or Infrared, Optical and Ultraviolet radiation (IR/Opt/UV). In their honor this feature is broadly referred to as the GZK-effect.

Another possible explanation with several supporters is that the cut-off represents the maximum acceleration energy from the cosmic accelerators. Depending on the presence or absence of detected CRs at higher than cut-off energies and the sharpness of the high-energy-end-dip, will determine whether the observed cut-off is due to the GZK effect or due to an inherent acceleration limit of their sources. In the former case there will be a contribution at energies slightly above the GZK limit from sources within the GZK horizon.

The high energy end of the CR spectrum is a point of reference for many theories. Although its complete determination remains inconclusive, the current definition of the highest energy limit and its overpass by future detected events can operate as a probe to new fundamental physics. This triggers the need for increased theoretical investigation but also simultaneously for experimental activity in the domain of EHECR physics. As already seen, to avoid the limitation of maximum acceleration imposed from astrophysical sources, models based on collapse/annihilation of topological defects and the decay of particle-relics of the early universe as an alternative way of extremely high energy CR production have been proposed and await experimental confirmation. To engage in the search of the derivation of further new fundamental physical mechanisms and the verification of the existed ones constitutes a remarkable field of astro-particle physics.

2.3.1 Composition models and CR flux spectrum

The chemical composition of ultrahigh energy cosmic rays remains an open question. Observational data indicate that extragalactic astrophysical accelerators are associated with protons and light nuclei as components of CRs whereas galactic accelerators are linked with the production of heavier nuclei components. Latest results from the Pierre Auger observatory indicate that there is a mixed composition of both light and heavy nuclei in the whole range of CR energies.

It is generally accepted that the CR components up to energies around the "knee" region are dominated by heavier nuclei thus indicating a Galactic origin. For this reason all the attention of high-energy astrophysicists studying the fundamental characteristics of CRs is directed to the above the "knee" part of the spectrum. Regarding that region, there is a tendency to lighter nuclei and protons for energies around $10^{18}eV$ and above implying that highest energy CRs are coming from extragalactic sources. It is to be expected that due to extremely low flux of high energy CRs, the accurate determination of their composition is notoriously difficult.

Since each source contribution corresponds to a different part of the spectrum, where it dominates, there has to be a specific region where a transition from Galactic to Extragalactic component occurs. Observing carefully the CR spectrum in Figure 2.2 it is clear that this region should be the "ankle" around $E \sim 3 \cdot 10^{18}eV$ as it is the only region where the spectrum gets harder, that is, it flattens. At that point the spectrum exhibits a smaller slope meaning more particles per energy range in comparison with lower or higher energies. This flattening should be due to both contributions of Galactic and Extragalactic sources. Results from other studies like the one of HiRes Collaboration suggest that the transition occurs in a region below the "ankle" called the "second knee" around energies of $5 \cdot 10^{17}eV$ where another kink in the spectrum is reported. This suggestion implies there might be CRs coming from extragalactic sources for energies lower than the "ankle" energies.

Accepting the certainty of the galactic origin CRs in terms of composition and energetics, the focus of all studies is on the composition of extragalactic CRs through simulations of their propagation. In these studies there are two opposite composition models for the extragalactic (EG) cosmic ray component. The first scenario assumes that the extragalactic origin CRs is consisted of pure protons only. In this scenario in order to fit the observational data propagation models suggest that the spectral index of the injected spectrum should have the value of 2,6 ($\sim E^{-2,6}$). The main problem facing this scenario is that there are no physical mechanisms that reproduce such an index. In this model the "ankle" is interpreted through an analogy with the GZK cut-off. As it is generally accepted at the high end of the cosmic ray spectrum, due to photo-pion production, the flux of the UHECRs is suppressed. An analogy exist in lower energies around $10^{17-18}eV$ where the pair production of proton interactions with the cosmic background ($p + \gamma \rightarrow p + e^- + e^+$) leads to a harder flux-energy spectrum. However, the interpretation of the "ankle" as a pair-production dip requires a very large fraction of protons at the source. This model is in favor of a Galactic-Extragalactic transition at energies below the "ankle" in the region of "second-knee". With this assump-

tion, the concern about the ability of galactic acceleration of CRs to energies up to the high end of the spectrum ceases. Proton composition models provide good fit data down to energies of $10^{18}eV$. Finally, assuming a broken power-law at injection for energies below and above the "second knee" can help avoiding an energetic problem for EG sources.

The second scenario assumes that the extragalactic origin CRs is consisted of a mixed composition of pure protons and heavier nuclei. In related propagation models it is assumed that the composition at the EG source is the same as the composition at a galactic source of lower energy. For this propagation model to fit the observed data an injection spectrum with spectral index of $2,2-2,3$ is required which corresponds to a harder spectrum with respect the one for pure proton case. Since both numerical and analytical studies of acceleration mechanisms in relativistic shocks, which was described as the most likely CR acceleration mechanism (DSAM), conform with a spectral index of $2,2-2,3$, this scenario overcomes acceleration limitations introduced by pure proton model thus taking the lead as the most reliable case.

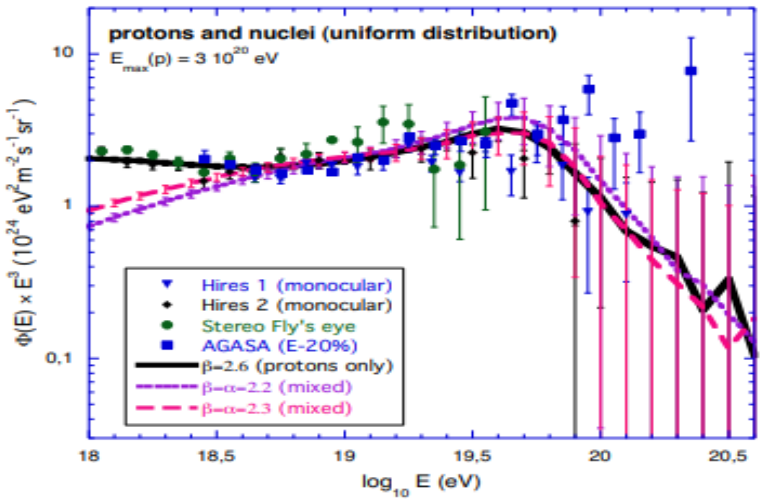

Figure 2.4: Cosmic ray propagation simulation spectrum for both composition models of pure proton and mixed nuclei. Experimental data points from HiRes, Fly's Eye and AGASA are included. A uniform distribution of sources is assumed.

Provided such injection index and reasonable fractions of proton component of the order of $40-50\%$ there is a good agreement between simulation models and observed data. For such proton fractions the standard interpretation of the "ankle" as the transition from GCRs to EGCRs is recovered.

More specifically, the transition occurs for energies slightly below the "ankle" at ends at the "ankle". On the other hand for the interpretation of the "ankle" as a pair-production dip to be viable in this case, the fraction of protons at the EG source cannot drop below 85%. For the GCR/EGCR transition to be explained more fundamentally, the extragalactic magnetic field should have a high enough (but reasonable) intensity to prevent lower energy CRs from reaching us from distant galaxies.

In Figure 2.4 the neutrino spectrum from the paper of Allard et al. ([10]) working on simulations of the propagated CRs for both composition models is shown. Additional experimental data from HiRes, Fly's Eye and AGASA are shown for comparison. A uniform distribution of the sources is assumed. For the pure proton case simulation data provide a good fit to the experimental ones down to energies of $10^{18}eV$ while in the mixed composition case there is an equally good agreement with the observed data down to energies of around $10^{18,5}eV$. The flaw of the former is that requires acceleration mechanisms not observed in astrophysical situations.

As it is evident from the above the two main aspects of the CR phenomenology, the injection spectral index β in order to fit the data and the GCR/EGCR transition in terms of the energy dependence from the "ankle" are closely interrelated.

Chapter 3

From UHECRs to cosmogenic neutrinos

In this chapter the interesting path from UHE cosmic rays to the production of cosmogenic neutrinos and the recording of their flux spectrum is unfolded step by step. In order to fully understand the cosmogenic neutrino field, this path must be faithfully followed. The beginning of the prominent path starts with the analysis of the UHECR interactions.

3.1 Interactions of UHECRs with photon background

It has been understood that when reference to high energy cosmic rays is made, what is essentially meant are only UHE nuclei that have been stripped out of their atoms ranging from the smallest, the hydrogen nucleus or proton, to nuclei of much heavier composition such as lead. For the study of UHECR interactions the two composition models described in section 2.3 are going to be examined separately.

The photonic background can also be treated as two separate parts, the one corresponding to the $2,7K$ primordial Cosmic Microwave background (CMB) and the one corresponding to the IR/Opt/UV background commonly mentioned also as EBL meaning the diffuse Extragalactic Background Light. EBL refers to all the accumulated radiation in the universe coming from star formation processes having also a contribution from AGNs. The IR/Opt/UV background evolves less than the CMB because unlike the latter it is continuously produced during the cosmic history. The decrease of this background with redshift is thus slower than the one of the CMB leading to a milder cosmological evolution.

3.1.1 Interactions of protons with photon backgrounds

In the CR composition scenario of pure protons the interactions during propagation are mainly with photons of the CMB which constitutes the densest background. Instead, interactions with the IR/Opt/UV have a much lower probability affecting only a small fraction of the propagating protons and in high energies are considered negligible. However the EBL background has a significant role in terms of interactions with secondary particles producing the desirable neutrinos. The most dominant interaction of pure protons is the photo-pion production off CMB and IR/Opt/UV photons. Photo-pion production is carried out through the Δ resonance referring to a family of subatomic particles that are consisted of three up or down quarks:

$$N + \gamma \rightarrow \Delta \rightarrow N^{'} + \pi^{\pm} \tag{3.1}$$

where N refers to a nucleon which in this scenario is the proton. In detail the following reactions take place:

$$p + \gamma \rightarrow n + \pi^{+} \Rightarrow \tag{3.2}$$

$$\begin{cases} \pi^{+} \rightarrow \mu^{+} + \nu_e \\ n \rightarrow p + e^{-} + \overline{\nu_e} \end{cases} \Rightarrow \tag{3.3}$$

$$\mu^{+} \rightarrow e^{+} + \nu_e + \overline{\nu_\mu} \tag{3.4}$$

Through the Δ resonance both secondary pions and neutrons are produced. Via pion decay secondary neutrinos are produced which are known as "cosmogenic". Cosmogenic neutrinos can also be produced through the beta (β) decay of the secondary neutrons being unstable as free particles with lifetime of the order of $881s$. The subsequent decay of the muon leads to a further production of neutrinos whose ratio of flavors $\nu_e : \nu_\mu : \nu_\tau$ corresponds to values of 1:2:0 without having taken into account the neutrino oscillations. Neutrino oscillation refers to the property where a neutrino although being identified with a specific flavor (lepton family number) it can be later measured as a neutrino with a different from the initial flavor. The photo-pion production through the Δ resonance has a 1/3 probability of isospin flip (change of an up or down quark to the opposite and subsequently a change from a proton to a neutron in this case) of the incoming nucleon with each isospin flip leading to the production of three neutrinos as described above. Delta resonance is a high inelasticity process corresponding only to 20% of the incoming proton energy being given to the secondary particles ($E_s = 0, 2E_p$). Its high interaction threshold of energies $E \sim 7 \cdot 10^{19} eV$ is

translated to the feature of high energy CR spectrum cut-off or otherwise known GZK effect.

Cosmogenic neutrinos can additionally be produced from the interactions of the secondary neutrons with the photon background. The detailed reaction chain is the following:

$$n + \gamma \rightarrow p + \pi^- \tag{3.5}$$

$$\pi^- \rightarrow \mu^- + \overline{\nu_\mu} \tag{3.6}$$

$$\mu^- \rightarrow e^- + \nu_\mu + \overline{\nu_e} \tag{3.7}$$

Though, the Delta resonance dominates multi-pion production with most of the neutrinos being produced close to energy threshold resulting to non many CR detected events above the GZK limit.

A neutrino production process which mostly dominates to lower CR energies is the pair-production process off CMB photons:

$$p + \gamma \rightarrow p + e^+ + e^- \tag{3.8}$$

producing electrons and positrons that continue the E/M cascade development. Pair production is associated with large energy losses of the incoming proton and dominates up to energies of $10^{18} eV$.

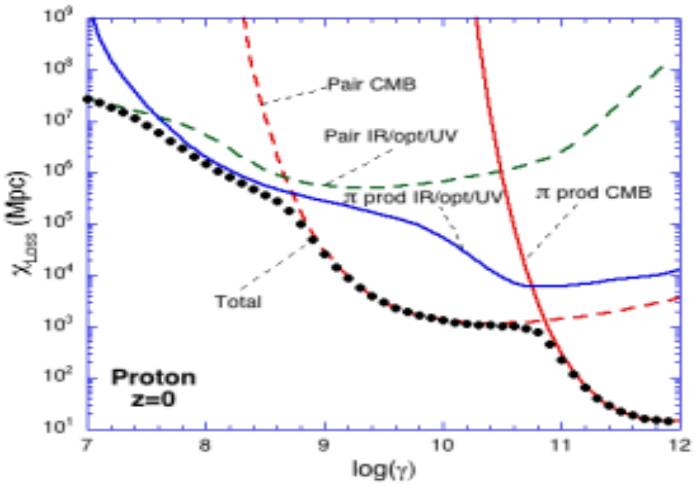

Figure 3.1: Attenuation length for different proton interaction processes. The logarithm of the horizontal axis refers to the Lorentz factor γ of the proton.

In Figure 3.1 of Allard et al. ([14]) the attenuation length expressing the distance needed to be covered from the proton in order for the probability to be "absorbed" by photon backgrounds to drop to the 1/e is shown for

the different proton interaction processes described above. Thus smaller attenuation length implies bigger probability for absorption. At lower energies the photopion production off IR/Opt/UV competes with the pair production process off CMB photons. It is clear that for the photopion production off IR/Opt/UV the attenuation length decrease in a smooth way and as soon as the pair production threshold with the CMB is surpassed at energies around $10^{18}eV$, the pair production becomes dominant and photopion production with IR/Opt/UV photons is neglected. On the other hand, at very high energies the attenuation length for the photo-pion interaction of pure protons with CMB photons decreases with an extremely steep way (happens when the energy threshold for photo-pion production is surpassed around $E \sim 7 \cdot 10^{19}eV$) meaning that this interaction dominates at the high end of the spectrum. Last, the propagated protons can lose a fraction of their energy due to adiabatic losses.

3.1.2 Interactions of nuclei with photon backgrounds

In the mixed CR composition scenario the most common interactions of UHECR nuclei during propagation are the photodisintegration or photoerosion processes. These nuclear processes refer to the situation where a UHECR nuclei absorbs a photon, gets excited and immediately decays by emitting one or more secondary nucleons and α particles. The interactions occur both in the CMB and the IR/Opt/UV backgrounds. The nuclear reaction is the following:

$$(A, Z) + \gamma \rightarrow (A - n, Z - n^{'}) + n \cdot N \tag{3.9}$$

where n($n^{'}$) represents the number of the stripped nucleons (protons). Since the energy required for these processes is much less than the rest mass of the nucleus, these processes are assumed to be elastic. The production of secondary nucleons will subsequently lead to their beta decay producing secondary cosmogenic neutrinos.

The photoerosion cross section is assumed to be proportional to the mass of the nuclei and to become dominant in different energies for different photoerosion processes. At the lowest energies a photodisintegration process called Giant Dipole Resonance (GDR) becomes dominant in cross section. GDR results in the emission of one or two secondary nucleons which in turn through a second interaction of beta decay or photo-pion production generate cosmogenic neutrinos. GDR processes are linked with a high cross section and the lowest energy thresholds ranging from an $\epsilon_{min} = 8MeV$ to around $20MeV$ with all energy scales being measured in terms of the nucleus rest frame. GDR process can be interpreted macroscopically in terms of excitation as a

two fluid system where a proton fluid vibrates against a neutron fluid.

Quasi-Deuterium or QD process is the dominat photoerosion process for energies ranging from around $30MeV$ up to the photo-pion energy threshold. In QD process a photon interacts with a nucleon pair within the nucleus, hence the name quasi-deuterium, resulting in the ejection of the pair and possibly additional protons or neutrons. QD process is comparable to GDR process but in contrast has an almost constant cross section and does not affect strongly the UHE nuclei propagation. The QD interaction threshold is given by: $\epsilon_{QD} = 33,6 \cdot A^{-1,6} MeV$ where A represents the atomic number of the nuclei.

Once the energy threshold for the photo-pion production is exceeded, photo-pion process or otherwise called Baryonic Resonance (BR) becomes dominant in the cross section. The energy threshold is estimated about $150MeV$ in nucleus frame or $5 \cdot 10^{21} eV$ in the lab frame. In this case nucleons either free, meaning that a first photodisintegration interaction to strip them out of the nucleus has already taken place, or bound-trapped inside the nucleus interact with the photon background to produce pions of all kinds (indirect and direct pion-production respectively):

$$N + \gamma \rightarrow N^{'} + \pi \tag{3.10}$$

where N represents this time a nuclei. After the photon interaction the bound nucleons are ejected outside the parent nucleus possibly interacting further with a nucleon pair resulting in further ejection of nucleons. Depending on the type of the baryonic resonance the photo-pion cross section features different peaks with baryonic resonances heavier than the first Δ to be much less pronounced that those described for nucleons. In general photo-pion processes of UHE nuclei have different cross sections in comparison with the ones for an UHE proton. Since the photo-pion production has taken place, the production of secondary cosmogenic neutrinos is carried out with exactly the same way as in the case described in subsection 3.1.1 regarding proton interactions, that is, through muon production and subsequent muon decay or a neutron decay.

Moreover, for energies exceeding the value of 1GeV photofragmentation (or otherwise being referred as photodissociation or photolysis) processes become dominant for UHE nuclei. As their name suggests, these processes break the nucleus into smaller fragments of significantly lower mass and energy. Excluding high energies ($E \geq GeV$) this process is subdominant in comparison with photoerosion processes.

Pair-production is also present for UHE nuclei with an energy threshold proportional to the mass of the nuclei and of the order of $A \cdot 10^{18} eV$. Only

a small fraction of the nuclei is lost thus considering the process as almost elastic. In nuclei case pair-production plays a secondary role as its mean free path is relative subdominant with respect to the aforementioned processes. Energy losses also occur due to adiabatic processes.

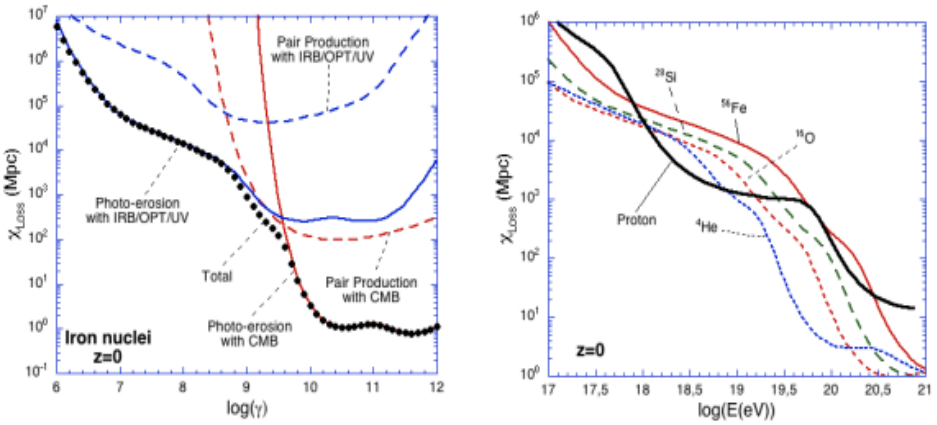

Figure 3.2: Left: Attenuation length for different interaction processes of an iron nuclei assuming zero redshift as a function of the logarithm of the Lorentz factor γ. Right: Attenuation length corresponding to different mass compositions of nuclei as a function of the energy.

In the left part of Figure 3.2 of Allard et al. ([14]) the attenuation length of an iron (Fe) nuclei for different interaction processes with the two types of photon backgrounds described above assuming zero redshift of the sources is shown. Photoerosion processes off IR/Opt/UV background are dominant in lower energies from which the GDR process off IR photons has the biggest contribution. Pair production off CMB competes these processes at intermedium energies and overpasses them for a very narrow energy range corresponding to iron Lorentz factor $\gamma \sim 10^{9,5}$. At higher energies ($\gamma \geq 10^{9,5}$) photoerosion processes off CMB are the dominant component of UHE nuclei interactions from which GDR process off CMB has the highest contribution at energies ranging from $\gamma = 10^{9,5}$ to $\gamma = 10^{10,5}$ while BR process off CMB dominates at energies over $\gamma = 10^{11}$. In the right part of the Figure 3.2 the attenuation length for different nuclei regarding all possible interactions is shown. As seen in the diagram the attenuation length for He (light nuclei) is much smaller than that of proton or Fe (heavy nuclei). As a consequence, light nuclei should not contribute as significantly as protons or heavier Fe nuclei at the high energy end of the spectrum.

3.2 Cosmogenic neutrinos/ Mechanisms of production

To study the most important features of cosmogenic neutrinos such as their flux spectrum and their maximum detectable energy, first an informative definition and a distinction with astrophysical neutrinos is necessary. It is very likely that every source of cosmic rays (referring to the charged component), for example a cosmic ray accelerator such as a black hole or GRBs emits also photons and neutrinos as secondary particles. The emission may come from the decay of pions which in turn may be produced in hadronic interactions of the CRs with material in or around the source. Another source of neutrinos may be the decay of supermassive metastable particles called X originating from physical processes in the early universe. Such processes are the decay of topological defects (TDs) referring to cosmic strings, magnetic monopoles etc. closely related with Grand Unified Theories (GUTs). X particles could also be long term remnants of the early universe that decay in the current epoch. Neutrinos produced through the above processes are called "astrophysical" neutrinos or "in situ" neutrinos.

On the other hand, "cosmogenic" neutrinos are those produced during propagation of UHECRs from their source to our observational instruments. Cosmic rays of ultra high energy interact with the photon backgrounds (either CMB or IR/Opt/UV) to produce neutrinos of all flavors as analytically described in the previous section. Cosmogenic neutrinos are also referred to as "off-situ" neutrinos and are produced via two principal channels: the decay of pion particles or the beta neutron decay with both types of particles being secondary particles produced by the UHECRs (of both composition models) interactions off CMB and IR/Opt/UV photons.

Protons, neutrons and heavier nuclei of UHE interact with the CMB and assuming lower energies with the more energetic IR/Opt/UV background to produce charged pions (BR processes). The relevant reactions of pion production are:

$$\begin{cases} p + \gamma \rightarrow n + \pi^{+} \\ n + \gamma \rightarrow p + \pi^{-} \\ N + \gamma \rightarrow N^{'} + \pi \end{cases} \tag{3.11}$$

Subsequent decay of those pions results in the production of muons:

$$\pi^{\pm} + \gamma \rightarrow \mu^{\pm} + \nu_{\mu}(\overline{\nu_{\mu}}) \tag{3.12}$$

which in turn due to small length scales decay to generate more neutrinos:

$$\mu^{\pm} \rightarrow e^{\pm} + \overline{\nu_{\mu}}(\nu_{\mu}) + \nu_{e}(\overline{\nu_{e}}) \tag{3.13}$$

In total 3 neutrinos, 2 neutrinos of flavor $\nu_\mu(\overline{\nu_\mu})$ and one neutrino of flavor $\nu_e(\overline{\nu_e})$, are produced via this charged-pion decay channel. The energy of the produced neutrinos is of the order of a few percent of that of the parent nucleus.

Neutrinos can also be produced by the pion production off photon backgrounds of the secondary nucleons produced via the first UHE proton-neutron-heavy nuclei interactions (GDR process). Due to the requirement of the presence of a first reaction this component of the charged-pion decay channel has a smaller probability to take place. At lower energies where interactions with the higher energetic IR/Opt/UV background take place, although the small interaction probability, due to steep UHECR injection spectrum (thus more particles being present at lower energies) the production of neutrinos is relatively high.

The second principal channel for neutrinos production is via the beta decay of neutrons:

$$n \rightarrow p + e^- + \overline{\nu_e} \tag{3.14}$$

which can either be free, being secondary neutrons from proton-photopion interactions or being ejected from a parent heavy nucleus due to photodisintegration processes. The final energy imparted to the produced neutrino from a heavy nucleus interaction process in this channel is of the order of a thousand of that of the parent nucleus.

Last, an alternative way of cosmogenic neutrino production is the decay of nuclei produced by photodisintegration processes:

$$(A, Z) \rightarrow (A, Z-1) + e^- + \nu_e \tag{3.15}$$

or

$$(A, Z) \rightarrow (A, Z+1) + e^+ + \overline{\nu_e} \tag{3.16}$$

In this case the energy imparted to the produced neutrino is very slightly above one thousand of the parent nucleus.

"Cosmogenic neutrinos" bear the information of UHECR sources and help scientists understand the objects and phenomena from which the latter are produced. By not being deflected by magnetic fields during propagation (as being uncharged) and thus preserving their energy, cosmogenic neutrinos are viable probes of the most fundamental characteristics of the UHECR sources up to high redshifts. Their contribution is characterized by the constraint of the UHECR sources' nature, distribution, chemical composition, injection spectrum and cosmological evolution. Due to their extremely low interaction rate, the majority of cosmogenic neutrinos arrive on Earth without initiating air showers in the atmosphere as CRs do. However, when interacting with

denser media such as water detector tanks, the sea water or the Antarctic ice a neutrino interaction is more likely to happen thus initiating a particle cascade leading finally to the emission of radiation. As will be seen in detail in the next chapter lunar observations searching for radiation produced when cosmogenic neutrinos interact with the dense medium of the outer layer of the Moon's surface consist a promising technique for neutrino detection.

3.3 Flux spectrum

Various studies have been conducted for the understanding of the neutrino flux spectrum and many attempts to depict it as close to observational data as possible. A detailed analysis of neutrino flux spectrum through observations or computational simulations can have a twofold interest. Depending on the characteristic neutrino flux shape throughout the energy range, useful conclusions on the sources of UHECRs can be drawn. On the other hand, these studies should act as a benchmark for the design of the key features of future experiments such as the sensitivity range of the upcoming next generation telescopes to neutrino fluxes.

Neutrino fluxes contain contributions from the overall universe as the missing horizon for neutrino propagation implies that neutrinos arrive from all directions. Thus neutrino fluxes from individual sources are washed out by a large isotropic background. Assuming no magnetic deflection (no neutrino charge) the only energy loss mechanisms are due to redshift and neutrino flavor oscillations. Cosmogenic neutrinos are assumed to travel almost freely through the universe. Focusing to neutrino fluxes coming from the universe and isolating them from those coming from the atmosphere can be achieved by observing neutrinos or conducting simulations only at high energies ($E \geq 10^{12} eV$). Detection of neutrinos at high energies can contribute to constrain the UHECR sources' distribution.

High-energy particle scientists have focused their interest on performing simulations of UHE cosmic ray propagation from cosmological sources and the subsequent derivation of neutrino flux spectra which can be used to effectively understand the observational data. The shape of the cosmogenic neutrino flux spectrum is highly dependent on some of the still unknown parameters of the UHECR sources such as the sources themselves, their cosmological evolution with the redshift, their injected composition spectrum (composition scenarios), the abundance rates of each energy range and lastly the maximum acceleration energy of their injected CR spectrum. Other factors that should be taken into account for the propagation model are the energy of the interacting photon background, the degree of inelasticity of the

interactions regarding the corresponding composition model and the energy losses due to universe expansion.

Since there are neutrino fluxes contributions from the overall universe the knowledge of cosmological evolution of both UHECR sources and the astrophysical backgrounds is essential for propagation simulation models. The source evolution models are distinguished in the following cases: a uniform evolution of the sources that corresponds to FRI galaxies (Fanaroff–Riley classification of radio galaxies), a subcategory of AGNs, evolution according FRII galaxies which is an optimistic scenario not in favored due to disagreement with observational data at highest energies, evolution according to the star formation rate which is a general indicator of matter density in the universe describing the rate at which gas and dust is turned into stars measured in solar masses per year and lastly evolution according to gamma ray burst (GRB) rate. Assuming that UHECRs are produced in astrophysical sources, the most natural source evolution scenario is the one corresponding to the star formation history. In terms of the background evolution, since the IR/Opt/UV background is continuously produced during the cosmic history, it should evolve less than the CMB and thus do not decrease as fast as the one of the CMB. Therefore there are different background contributions from different redshifts depending on the chosen type of background.

As far as the compositions of the sources are concerned, these correspond to the two known scenarios of pure protons and mixed composition of UHE nuclei with a predominant and varying percentage of photons. It is assumed that the composition does not vary from the injection point until the point where the interactions with the photon background take place.

The maximum acceleration energy is a factor of large uncertainty as it is dependent on the nature of the sources, their energetics and several relevant parameters such as the CR escape time and the energy losses due to the corresponding model interactions. For the proton case the maximum acceleration energy is usually considered to be around $10^{20-21}eV$, that is, over the limit of photo-pion production cause otherwise a low $E_{p,max}$ would lead to a drastic suppression of the neutrino flux . For the mixed composition case the maximum acceleration energy is proportional to the one of proton case and to the atomic number of the nuclei:

$$E_{max} = Z_i \cdot E_{max}(H) \tag{3.17}$$

where Z_i is the charge number of the given nucleus i. This assumption is acceptable as confining the particles to the source limits the maximum acceleration energy.

Under the assumptions that UHE neutrinos do not have any losses due to universe expansion and do not interact with particles of the interstellar

medium or the atmosphere, their flux spectrum has a general shape for all possible combinations of the aforementioned cases of each separate parameter characterized by two (plus one at lower energies) bumps. There is a high energy peak at energies around EeV or $10^{18-18,5}eV$ due to interactions with the CMB. At high energies (EeV) although the interaction probability is much higher, due to the small number of the interacting particles the peak has smaller amplitude than the one corresponding to the lower energy peak. The latter occurs at intermedium energies of the order of PeV ($10^{14,5}eV$) due to interactions of the UHECRs with the IR/Opt/UV background. At lower energies the number of the interacting particles is much higher (due to deep injection spectra generated by the acceleration mechanisms) and thus despite the low interaction probability the peak has larger amplitude. The positions of the peaks differ for each individual combination of parameters and strongly depend on evolution of the interaction probability and the injection spectrum. Furthermore the neutrino fluxes can vary of many orders of magnitude throughout the whole energy range.

In reality neutron beta decay is responsible for the appearance of a third peak in the spectrum at lower energies of the order of $10^{12,5}eV$ due to kinematics of the process. Moreover since the energy of the secondary cosmogenic neutrinos is at least an order of magnitude lower than the energy per nucleon (E/A) of the primary particle, it is clear that the neutrino fluxes are expected to be the lower the heavier the composition of the primary particles is.

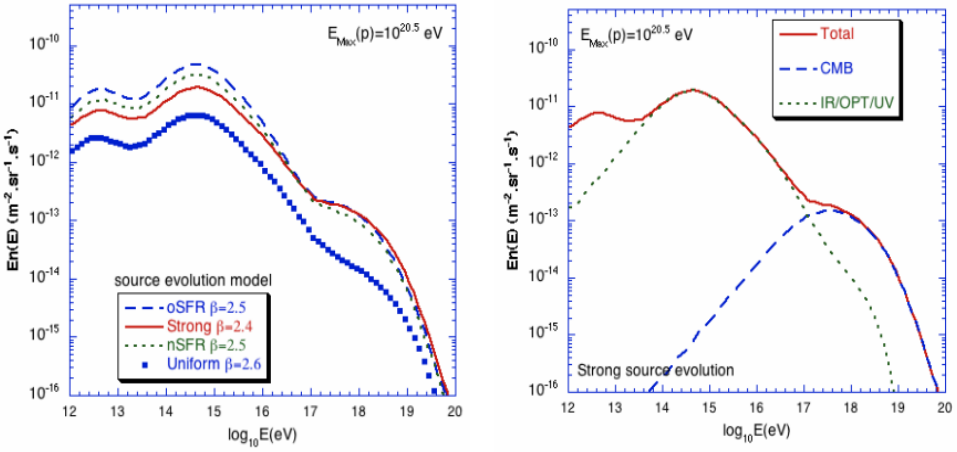

Figure 3.3: Left: Neutrino flux spectrum for a pure proton composition considering different evolution models for the UHECR sources. The maximum acceleration energy is $E_{p,max} = 10^{20,5}eV$. Right: Contribution of different backgrounds to the neutrino fluxes assuming a strong evolution case for the UHECR sources and the same maximum acceleration energy.

In the left part of Figure 3.3 of Allard et al ([14]) the neutrino flux for the pure proton composition scenario assuming maximum acceleration energy $E_{p,max} = 10^{20,5}eV$ and different evolution scenarios is shown. Injection spectral indices vary according to the source evolution scenario. The classical aforementioned neutrino flux shape with the three maxima and their corresponding magnitudes is clearly evident in the diagram. In addition it is clear that the flux shape spectrum do not vary significantly from one evolution scenario to another but there are significant deviations of its scale specifically for the uniform evolution case being an order of magnitude lower than the rest of the evolution models.

On the other hand, the right part of Figure 3.3 of [14] exhibits the contribution of different backgrounds to the neutrino fluxes assuming a strong evolution case for the UHECR sources. At lower energies the appearance of the third maximum is mainly due to contributions from proton interactions off the higher energetic IR/Opt/UV background and the subsequent beta decay of the produced secondary neutrons. Due to the hardening of the CR spectrum at these energies, more particles are possible to interact with the photonic background leading to higher amplitude peaks. This also applies to the intermediate energy maximum which corresponds to the highest amplitude of the spectrum. The intermediate maximum is attributed to photo-pion interactions of proton energies close to the interaction threshold around $10^{16}eV$. Assuming the energy of the produced neutrinos is of the order of a few percent of that of the initial proton the intermediate peak occurs at an energy of the order of $10^{14,5}eV$. At high energies the major contribution comes from photo-pion interactions with the CMB for energies close to the proton-CMB threshold resulting in a peak of lower amplitude around energies of $10^{17,6}eV$ due to softening of the proton spectrum at such high energies.

In the left part of Figure 3.4 of Allard et al. ([14]) the neutrino flux for the mixed composition scenario assuming maximum acceleration energy $E_{max} = 10^{20,5}eV$ and different evolution scenarios is shown. Again injection spectral indices vary according to the source evolution scenario. At high energies there is a great resemblance with the proton case neutrino spectrum, as the mixed composition is always highly proton enriched, with the peaks occurring at the same energy positions. The high energy peak is attributed to nuclei-photopion production off CMB while the intermediate one to interactions of heavier than proton nuclei with CMB. Finally the low energy peak being attributed to secondary neutrons beta decay, with the latter having larger contribution from nuclei rather than proton interactions with the IR/Opt/UV background, has been shifted to lower energies. Therefore overall there is a difference between the shape of neutrino flux spectrum for pure proton and mixed

composition cases.

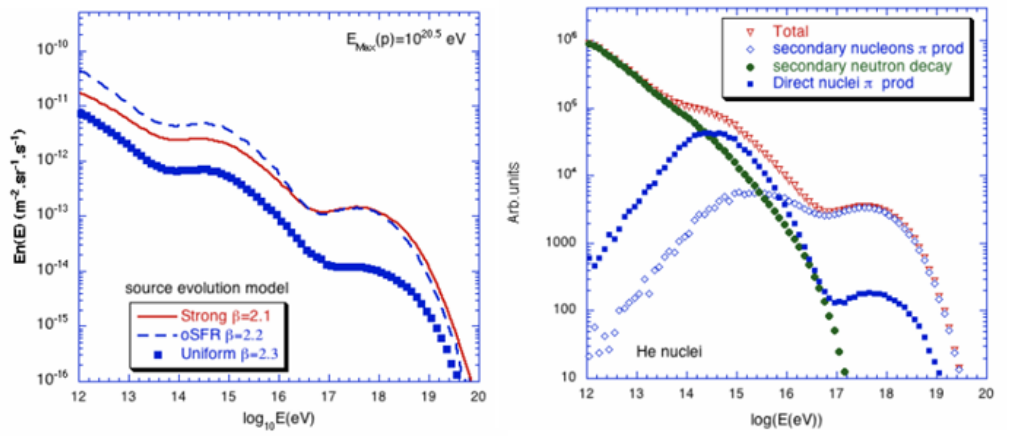

Figure 3.4: Left: Neutrino flux spectrum for a mixed composition considering different evolution models for the UHECR sources. The maximum acceleration energy is $E_{max} = 10^{20,5} eV$. Right: Contribution of different interaction processes to the neutrino fluxes measured in arbitrary units for a He nuclei assuming a strong evolution case for the UHECR sources and the same maximum acceleration energy.

In addition, in the right part of Figure 3.4 the contributions of different neutrino production processes to neutrino fluxes for the helium (He) nuclei assuming a strong evolution scenario are shown. At high energies the contribution of the secondary nucleon pion production (two interactions in total for the produced pion) dominates. Produced by GDR or QD processes the secondary neutrons interact with the CMB to produce charged pions which subsequently decay to give off neutrinos. At lower energies, neutrino flux produced by secondary nucleon photo-pion production drops faster (lower probability for the two required interactions to happen) than in the free nucleon case. The second peak is dominated by direct nuclei pion production as in this energy range the abundance of nuclei is much larger than that of higher energies. Neutron decay neutrino production takes over at lower energies as the energy threshold for neutron production from GDR photoerosion processes is decreased due to the energy per nucleon ratio dependence.

The predicted neutrino spectrum from simulation models show that the majority of neutrino fluxes are in general far from the sensitivity of many experiments searching for neutrino detection as most of them have sensitivity limits exceeding $10^{17} eV$. In section 4.4 lunar observation neutrino limits

from all the past and future experiments will verify this assertion. Icecube, Auger, ANITA and JEM-EUSO are the most promising experiments for neutrino detection having sensitivity limits that include the higher part of the spectrum. These experiments are using ground and underground particle arrays, flying ballons or space missions to search for direct neutrino detection or indirect through the detection of Cherenkov light, fluorescence light etc. In contrast fluxes at lower energies are not as close to the instrumental sensitivity as they are at high energies.

These promising experiments can provide important information about the UHECRs and their sources by the detection or not of UHE cosmogenic neutrinos. The non detection of cosmogenic neutrino events can put severe constraints in the nature and evolution models of UHECR sources. In contrast, a positive detection of UHE neutrino events can be useful to constrain the source composition models and the scenarios behind the transition point between Galactic and Extragalactic CRs.

The Argos telescope being introduced in the following chapter based on the feedback of the experimental results for neutrino fluxes and the sensitivities of current and past experiments will adjust its sensitivity limits in a way that will provide useful conclusions for the better understanding of UHECR sources and subsequently the early universe.

Chapter 4

Lunar observations

4.1 Askaryan effect

Dagkesamanskii and Zheleznykh in 1989 were the first to propose and develop the idea of lunar observations, namely that observing the moon with ground-based radio telescopes could yield the detection of radiation called "Cherenkov radiation" or "Askaryan effect" originating from particle cascades initiated by neutrino interactions with the outer layer of the lunar surface, called the "regolith". Lunar regolith basically refers to the outer layer of pulverized rock on the Moon's surface. The idea emerged naturally from the pressing need to find a solution to the problem of the non presence of a large volume detector for detecting the elusive UHE cosmic rays and neutrinos and was relied on the Askaryan's claim back in 1962.

Askaryan was the first to describe how a particle cascade created due to interactions of the incoming UHE particles in a dense medium produces coherent Cherenkov radiation. More specifically, Askaryan effect refers to the phenomenon whereby a UHE particle traveling faster than the phase velocity of light in a dense dielectric medium produces a shower of secondary charged particles leading to a charge-anisotropy and thus emits a cone of coherent radiation in radio or microwave part of the E/M spectrum. The phenomenon is quite similar to Cherenkov radiation in which case a charged particle moving with a velocity exceeding the velocity of light in that medium produces E/M radiation with a ring-like structure. The effect has been observed in silica sand, rock salt, ice, water, the Earth's atmosphere (air showers) and is of primary interest in using bulk matter detectors. There are several detection techniques that can be implemented through experiments either using huge water tanks such as HAWC or Super-Kamiokande, the sea water such as the NESTOR experiment near Pylos in Greece, the Antarctic ice such as ANITA

and Ice-Cube or resort to lunar observations such as GLUE, NuMoon and LUNASKA.

For lunar experiments the cascade is created due to interactions of the UHE neutrinos with the nucleons and electrons in the lunar regolith. Neutrinos, if gravity doesn't take into account because of neutrino's small mass, as being uncharged interact only via the weak force. Thus the interaction cross sections are much smaller than those of other particle species such as electromagnetic processes with a photon. Due to the extremely small size of neutrinos with respect to atomic nuclei, the probability of a neutrino to hit them would be infinitesimally small but in materials consisted of much heavier nuclei such as the lunar regolith, the probability for the neutrino to come closer to them and subsequently interact with them increases steeply. At UHE the neutrino–nucleon cross-section is such that neutrinos traversing the lunar diameter are severely attenuated.

The neutrino interacts with matter through its wearer particles W^+,W^- and Z_0. Neutrino interactions can be classified according to whether they are charged or neutral current, nucleonic or leptonic depending on the interacting partner particle (with the nucleonic cross section to be larger in general than the leptonic one) and whether there is an exchange of energy or not. The basic discrimination though is to charged-current (CC) and neutral-current (NC) depending on whether a charged or a neutral particle is produced. The former is when neutrino exchange $W^{\pm}$ with nucleons while the latter is when neutrino exchange Z_0 with nucleons. The neutrino interactions can be conceptualized better from the Feynmann diagrams for neutrino-nucleus interactions below:

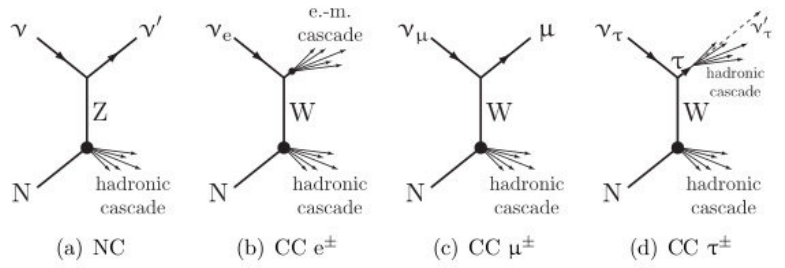

Figure 4.1: Feynmann diagrams for neutrino-nucleus interactions

These interactions may initiate two kinds of showers. Electromagnetic showers are initiated only by e^-/e^+ produced in $\nu_e/\overline{\nu_e}$ CC interactions (see b of Figure 4.1) as the Bremsstrahlung photons produced by μ and τ which in turn are produced by ν_μ/ν_τ CC interactions (c and d parts of Figure 4.1) won't have sufficient energy to initiate such a shower. Contrary hadronic

showers appear in both charged and neutral interactions. Most times a neutrino interact with a proton or neutron as a whole but if it has enough energy can also interact with the quarks inside the nucleon. In the case of CC, the interaction is "quasi-elastic" when the nucleon changes but do not break up. Examples of the CC interactions are:

$$\nu_\mu + n \rightarrow \mu^- + p \tag{4.1}$$

which is a CC μ^- interaction and

$$\nu_e + n \rightarrow e^- + p \tag{4.2}$$

which is a CC e^- interaction. Neutrinos generate charge excesses in hadronic showers. The charge excess can be justified since positrons tend to disappear through their annihilation into photons and further, electrons are created via Compton scattering by photons. As it is analytically explained in section 4.6 all contributing neutrino showers are assuming to occur in the lunar regolith near the surface with a fixed index of refraction.

Askaryan emission is radio emission due to the time variation of the net charge in the shower front. Although time variation of the total charge seems to violate the fundamental law of charge conservation, charge is totally conserved due to a positively charged plasma created behind the shower.

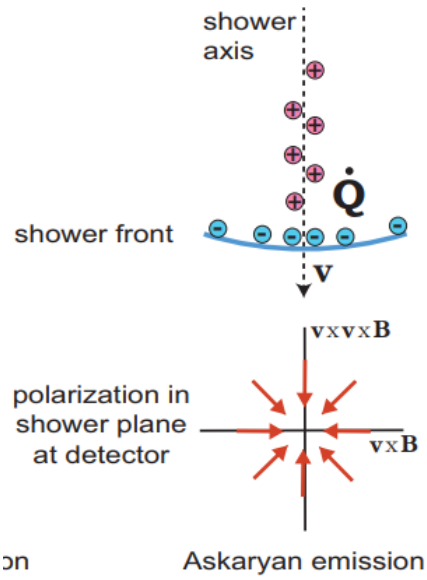

Figure 4.2: Polarization and net charge excess of Askaryan emission

The percentage of electron predominance can vary between $20 - 30\%$. Giving a simplistic picture of the phenomenon would be to simulate the net charge excess as a point charge whose strength alters with time and thus as a natural consequence has electric field lines that point radially. Therefore Askaryan emission is radially polarized and zero in the center at the shower axis. This also explains why the radio emission has a ring-like structure around the shower axis in dense media. This ring is called the "Cherenkov ring" and has a diameter that corresponds to the Cherenkov angle for that medium given by the relation:

$$\theta_C = arccos(\frac{1}{n_r}) \tag{4.3}$$

At that angle radio waves and ultra relativistic particles propagate roughly at the same speed.

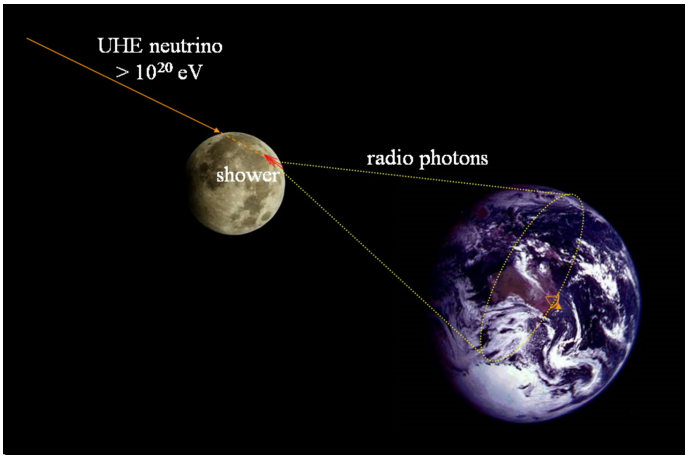

Figure 4.3: Ring-like structure of lunar radio signals emitted due to interactions of UHE neutrinos in the lunar regolith

Due to Cherenkov emission geometry and refraction at the lunar surface the radio signals reaching the Earth appear to originate almost entirely from the limb of the Moon. At the limbs of the moon neutrinos have less distance to cover in the dense medium and thus the expected event rates are higher. This effect is known as "limb brightening".

The lunar regolith being a radio transparent medium assists in letting the radiation escape as it is refracted by the Moon's surface (while a significant fraction is lost due to internal reflection) and reach Earth based detectors that remotely detect it as a narrow pulse of a few nanoseconds duration, corresponding to decimeter and greater wavelengths. Lunar radio pulses

from are much shorter in duration than any signals normally encountered in radio astronomy.

In order to determine whether a particular ray will eventually escape total internal reflection on the lunar surface, it is crucial to know the angle at which the ray meets the surface from the internal side of the moon and the scale of the surface roughness. Thus including the effect of surface roughness may change the angle of the internal refraction leading to a different result in terms of the "survival" of the radio pulses. Overall as seen in the following figure from Gayley et al ([35]) favorable tilts in the surface increase the fraction of the escaping rays for downwards neutrinos, which are defined as the neutrinos whose Cherenkov cone face downwards, to a larger degree than the unfavorable tilts reduce it.

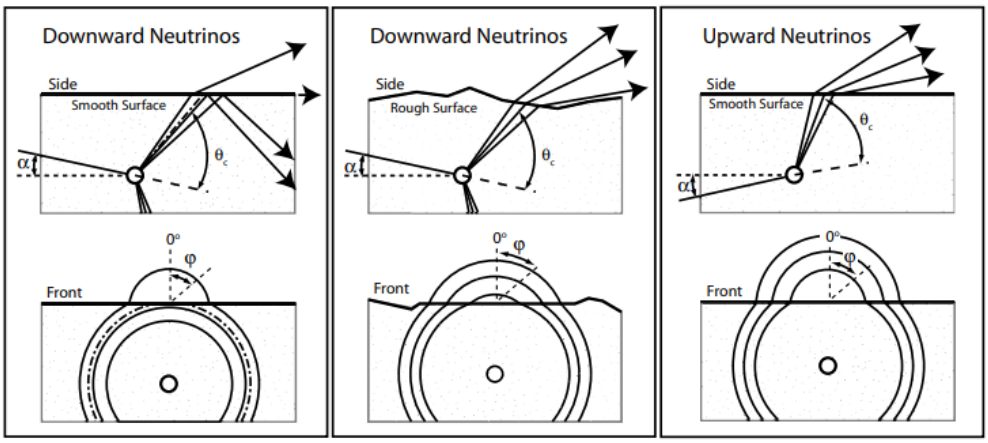

Figure 4.4: The Cherenkov cone viewed from the side and face-on both for upwards and downwards directed neutrinos incident on a smooth and tilted lunar surface

Surface roughness plays also an important role for neutrinos that have managed to survive a significant secant of the lunar regolith and thus, as facing upwards, interact with the rock producing a Cherenkov cone with a corresponding direction. These neutrinos are called upwards neutrinos. The complement of the angle of the initial incident neutrino angle to the normal is denoted as α in the depicted scheme in figure 4.3 and is positive for upwards neutrinos (to find the angle we follow the clockwise direction) while being negative for downwards neutrinos (following counterclockwise direction). For energies close to the GZK regime, both upwards and downwards neutrinos contribute in comparable amounts to the detection rate.

4.2 Radio detection

Radio detection in general is a promising technique for detection of ultra-high-energy neutrinos. Corresponding to a threshold of about 100 PeV, radio technique now stands equally alongside traditionally established techniques such as particle detectors for the study of the highest-energy galactic and extragalactic particles of all types. More specifically can compete with other techniques in precision for the reconstruction of important parameters of the tracked particles such as the initial energy and their arrival direction. The accuracy of a radio experiment can become optimum in combination with a complementary particle detector.

Coherent Cherenkov emission in the radio regime from neutrino- induced showers in the radio-transparent lunar regolith provides a viable mechanism for achieving a large enough detector volume for detection of the highest energy neutrinos. It is clear that as larger the aperture is, the greater will be the possibility of detecting an event, or in the case of none detections the more decisively constraining will be the inferred upper limit for detection.

There are several parameters though that can affect the detectability of the lunar radio pulses. Firstly, it should be pointed that the expected signal is broadband up to a cut-off frequency of $\sim GHz$ and is beamed in the forward direction of the particle shower. Its short duration is not longer than a few oscillations of the relevant frequencies. Parameters such as the field of view referring to the amount of the moon surface that our telescope captures, the telescope's total bandwidth coverage which should be within the desired range and its effective aperture defined as the product between the total collecting area and the aperture efficiency ($A_{eff} = A_{phys} \cdot e_a$) have a leading role in the particle detection.

The narrow time duration characteristic of the pulse indicate that the pulse is smeared out in time and that to be detected requires nanosecond time resolution. The pulse is dispersed as it passes through the Earth's ionosphere, which extends itself from about 60 km until more than 2.000 km in high, having also its amplitude reduced. Electron presence is the main factor that affects dispersion. During the day, sun radiation causes ionization of neutral atoms producing free electrons and ions. On the other hand, during the night, the recombination process prevails, where free electrons are recombined with ions to produce neutral particles. Therefore depending on the time of day, the slant angle of our telescope and the solar magnetic activity cycle, the total electron content referring to the electron column density, measured in gr/m^2 and being denoted as STEC, varies in time. Typical values range between 5 and 100 TECU where $1TECU = 10^{16} electrons \cdot m^{-2}$.

The dispersion delay of a pulse which expresses the delay in time arrival of different components of the pulse each corresponding to a different frequency is a frequency dependent quantity. The delay interval is also strongly dependent to the electron column density described above, which is also known as dispersion measure (Dm) officially defined as the integrated column density of free electrons between the terrestrial telescope and the Moon. Its formula is given by:

$$\Delta t = 1,34 \cdot 10^{-3} STEC\big(\frac{1}{f_{min}^2} - \frac{1}{f_{max}^2}\big) \tag{4.4}$$

corresponding to relation (1) of James et.al. ([28]) with minimum and maximum frequencies of the experiment's bandwidth to be measured in Hz and the STEC measured in $e^- \cdot cm^{-2}$.

Dm manifests itself observationally as a broadening of an otherwise sharp radio pulse. The prior knowledge of ionospheric dispersion can de-disperse the pulse before detection but it requires an accurate measurement of the TEC. Furthermore real-time de-dispersion can maximize the signal to noise ratio but requires the fastest hardware available.

Noise is one of the most influential factors in our measurements. Using separated bands with a different frequency range could lead to elimination of the terrestrial radio frequency interference (RFI). The discrimination procedure is much easier in a radio quite site. An example of such radio quite site is Skinaka's Observatory in the mountain of Psiloritis in Crete, a site that is inextricably linked to the experiment under study. For multi beam receiver RFI is distinguished from lunar pulses using anti-coincidence criteria, that is, by simultaneous detection of a pulse in all bands since they do not suffer ionospheric dispersion. Discrimination of local RFI can be achieved with a better accuracy if the experiment uses a pointing configuration with an off-moon beam (see Figure 4.5) being effective in detection of RFI pulses. Therefore proper trigger schemes are needed to balance the sensitivity of the telescope with the ability to exclude unwanted interference.

The dispersion measure also affects the procedure of data storage as it is a measure of the minimum sampling rate for detection of delayed pulses in different antennas. Due to the small Earth-Moon distance ($d = 3.844 \cdot 10^8 m$ on average), the delay in different antennas will be noticeably smaller with respect to other more distant astrophysical targets for radio detection. To effectively cover the broad bandwidth the pulse detection should be implemented in real time but the data should be stored for later processing as they exceed current computer capacity (storage limitations). A data discarding strategy would be essential for reducing raw data and could be achieved provided cutting edge technology hardware and suitable trigger logic thus

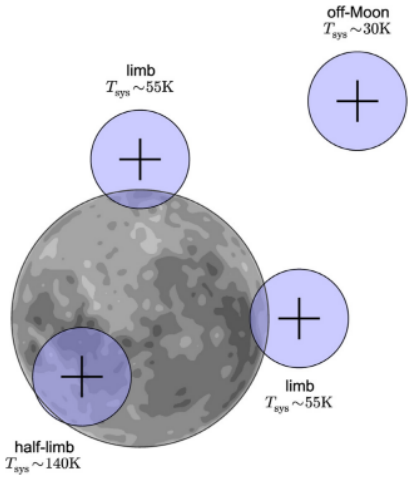

Figure 4.5: Noise from different pointing directions at the lunar surface

achieving real time detection. With real-time processing the receiver amplifies the signal and after down-converting it to lower frequencies and digitizing it, it passes through a finite impulse response filter and is checked for satisfying or not the threshold test and anti-coincidence criteria. In the former case the data is being stored for further processing.

Finally, the use of dual polarization in the receiver can significantly increase the possibility of detection of a pulse whose polarization is arbitrary. The polarization could be either linear or circular.

Having defined the parameters that deeply influence the ability to detect a coherent lunar short duration pulse, the reconstruction of the initial characteristics of the tracked neutrino is the next step of the procedure. The neutrino direction is accessible by measuring the light-arrival time in the individual antennas while integrations of the measured signals strengths provide a measure for the energy of the neutrino initiating the cascade.

Experiments that follow a specific method, in our case radio detection, to achieve their goal cannot remain unaffected by uncertainties in the steps of their implementation process which in turn inevitably lead to uncertainties in their measurements. The existence of uncertainties concerns the management of parameters such as the neutrino interaction cross section, the form of the structure and the extent of lunar surface roughness, the properties of the neutrino-producing shower and the degree of neutrino and radio pulse transparency at various depths in the lunar regolith. These uncertainties in some cases could lead to large deviations in the prediction models for the neutrino fluxes since the results strongly depend on the assumptions made, whether optimistic or pessimistic.

4.3 Sensitivity of radio telescopes to lunar origin coherent pulses

The sensitivity of radio telescopes to coherent pulses of lunar origin is deeply related with several parameters. One of the most crucial is the effective observing time t_{obs} corresponding to the effective time spent observing the moon having first excluded the so called "dead time" while data storage and RFI elimination. Additionally, there is a great dependence on factors such as the observing frequency v corresponding to the central frequency of the triggering band and the effective limb coverage ζ which is given as the product of the fraction of the circumference of the lunar limb within the beam multiplied by the numbers of beams of the telescope (when there are over than one) pointing at different parts of the limb.

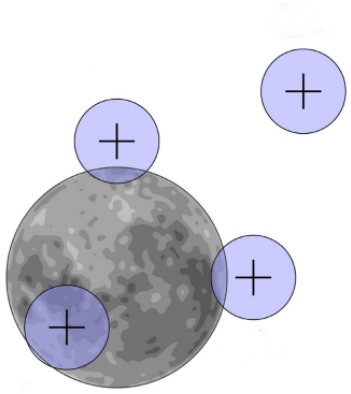

Figure 4.6: Pointing configuration scheme including different beams pointing at different parts of the lunar surface

Typically in many experiments with a pointing configuration that is consisted of several different pointing directions (beams pointing at the center, at half limbs, slightly off the moon) a single telescope beam covers only a part of the moon and the combination of all of them should be taken into account.

The sensitivity of a lunar experiment to detect a coherent radio pulse can be expressed in terms of a quantity called the minimum electric field strength ϵ_{min} measured in $V/m/Hz$ which express a threshold above which an Askaryan pulse of lunar origin could be detected on Earth. Taking into account the thermal noise that might increase or decrease the pulse amplitude, ϵ_{min} should be better considered as the level at which the detection probability is 50% instead of a pure absolute threshold.

Resorting to Bray's paper ([33]) the analytic formula for the derivation of the minimum detection threshold is:

$$\epsilon_{min}(\theta) = f_C \frac{n_\sigma}{\alpha} \sqrt{\frac{\eta}{B(\theta)}} \epsilon_{rms} \tag{4.5}$$

where ϵ_{rms} is the root mean square (RMS) spectral electric field strength for a particular bandwidth defined as:

$$\epsilon_{min} = \frac{E_{min}}{\Delta\nu} \tag{4.6}$$

where in turn E_{rms} is the spectral electric filed strength corresponding to a single polarization. Resorting again to Bray's relation (5) of:

$$E_{rms} = \sqrt{\frac{kT_{sys}Z_0\Delta\nu}{A_{eff}}} \tag{4.7}$$

we conclude for the ϵ_{rms} to the final expression:

$$\epsilon_{rms} = \sqrt{\frac{kT_{sys}Z_0}{A_{eff}\Delta\nu}} \tag{4.8}$$

In this expression T_{sys} stands for the system temperature which consists of various distributions. T_{sys} is a measure of the amount of noise that appears in a measurement and which the signal from the source (measured as antenna temperature) needs to stand out from to be detected.

Thermal emission from the moon dominates the contributions with an additional significant contribution from galactic background Synchrotron emission at lower frequencies and a third contribution due to internal noise of our telescope (T_{inst}). The parameter Z_0 stands for the impedance of free space with a fixed value of 377Ω, $\Delta\nu$ stands for bandwidth and k is the Boltzmann's constant. Last, A_{eff} represents the effective aperture of our Argos telescope defined as the product of the total collecting area of the telescope times the aperture efficiency

$$A_{eff} = A_{phys} \cdot e_a \tag{4.9}$$

In the analytic definition for ϵ_{min} above f_C accounts for the improvement in sensitivity from combining C independent channels with a significance threshold of n_σ in each which in turn expresses a significance level for exclusion and acts as a proportional constant to ϵ_{min}. $B(\theta)$ is the beam power (a measure of the amount of energy input per unit time) assumed to be radially symmetric, that is to have the form of an Airy disk, at an angle θ

from its central axis having a normalization of $B(0) = 1$. As one can easily deduced from the presence of the factor $B(\theta)$ in the calculation for ϵ_{min}, the minimum spectral electric field strength of a coherent pulse is calculated for each pointing separately assuming there is a multiple pointing strategy in the experiment.

The parameter η refers to the ratio between the total pulse power and the power in the chosen polarization channel. For linear polarization of the receiver the value of the parameter is equal to $\frac{1}{cos^2\phi}$ where ϕ is the angle between the incoming pulse and the receiver whereas for a circular polarization in the receiver takes the fixed value of 2 as mentioned in relation (9) of Bray's paper ([33]). Finally the α variable represents the proportion of the original pulse amplitude that has been recovered using several techniques to account for amplitude loss. The loss can either arise while converting the incoming analog pulse to digital samples or due to the phase of $\frac{\pi}{2}$ of the Askaryan pulse resulting in a bipolar pulse profile with amplitude splitting between the poles. An important amplitude loss factor can also be an inefficient sampling rate while data storage. All the aforementioned parameters have been analytically calculated in section 4.6 as part of the aperture determination process.

The detection sensitivity is furthermore highly directionally dependent. Therefore to be able to detect the fingerprints of neutrinos, telescopes should be pointing at specific astrophysical targets in the sky from which we expect to act as neutrino generators. Through their Cherenkov light cone produced in the lunar surface and based just on geometry, the reconstruction of their initial direction can be implemented and thus identify their origin (see Figure 4.3).

4.4 Neutrino flux limits from past and future experiments

Lunar observations is a field that in the past attracted the interest of many scientists with the first attempt to be recorded in 1995 from Hankins et al ([23]) using the 64m Parkes radio telescope followed by GLUE and Kalyazin experiments. More recent successful experimental attempts were made by LUNASKA, ATCA, NuMoon, RESUN and LORD. The most promising of these is considered to be the upgraded LUNASKA experiment planned to be operated with the upcoming next-generation SKA telescope currently being constructed in Western Australia and South Africa. The SKA is expected to have completed both construction phases by 2030 with its final phase cover-

ing approximately a total collection area of 1 square kilometer. Most of the current neutrino radio experiments are in the prototype phase aiming to the first detection of a neutrino event. Older experiments though remain exceptionally useful as old estimates can be used by scientists to scale sensitivities for upcoming experiments.

The primary goal for lunar Cherenkov experiments is to produce UHE neutrino flux limits as a function of the incoming neutrino energy. In order to determine these limits, each individual experiment has developed its own independent method of calculation of its sensitivity and its effective aperture to radio pulses. For most of the aforementioned experiments the corresponding limits on the diffuse neutrino flux are shown in the figure of [33] below.

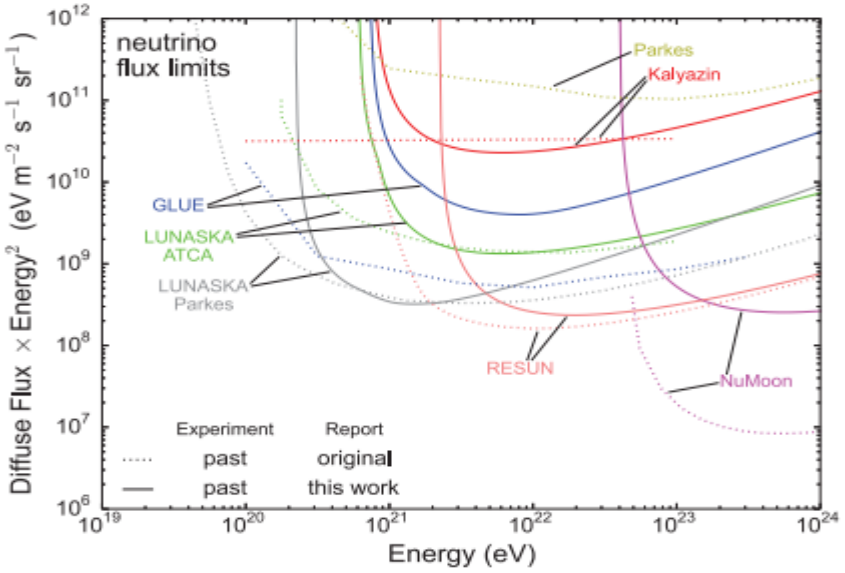

Figure 4.7: Limits on the diffuse neutrino flux set by past experiments such as Parkes, Kalyazin, GLUE, LUNASKA, RESUN and NuMoon both from their original calculation procedure and from the analytic method of Gayley et al.

Figure 4.7 shows both the limits derived from the original work on their calculation and also the limits from the work of Bray ([33]), based on the analytic method of Gayley et al ([35]) for the effective aperture calculation that we also follow in this work. The analytic formula shows that the limits are eventually less sensitive to neutrino fluxes than previously believed (more right in the diagram). In general all the experiments whose limits are depicted in the diagram are little to no sensitive at all to neutrinos in the range of energies close to the GZK cut-off which is estimated around $10^{19,6}eV$. On

the other hand they all are sensitive to neutrinos of much higher energies up to $10^{23-24}eV$. The detection of an UHE neutrino at energies higher than $3 \cdot 10^{20}eV$ which corresponds to the detected events verified from the Pierre Auger Observatory and are the highest energy detectable events observed so far, would pave the way for the establishment of new physics or for the verification of already existing "exotic" models.

Using data publicly available for past and future experiments and reproducing them following step by step the analytic formula of Gayley et.al ([35]), we produced the following figures depicting first (Figure 4.8) past experiments considering different pointing beams in each such as GLUE, LUNASKA , NuMoon and then (Figure 4.9) a mix of past and future experiments for a better comparison.

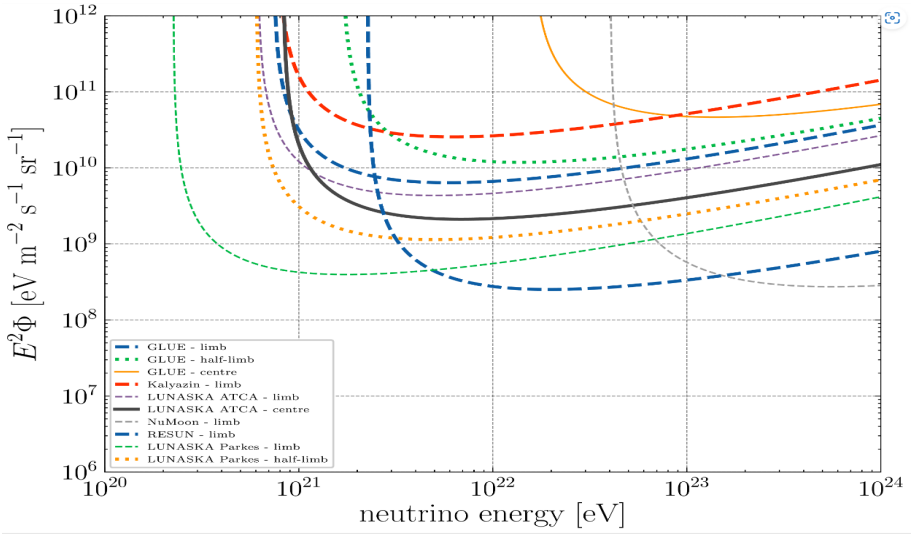

Figure 4.8: Limits on the diffuse neutrino flux set by past experiments such as Parkes, Kalyazin, LUNASKA ATCA, LUNASKA Parkes, RESUN and NuMoon from reproducing publicly available data and using the analytic method of Gayley et al.

It is evident from the above and below figures that the results of our analytic work for past and future experiments are consistent with the aforementioned claim that lunar experiments are weakly sensitive or non sensitive at all to cosmogenic neutrinos. Their range of detection energies acts as a weapon to prove ambitious scenarios for new experimentally-unconfirmed mechanisms for the production of far higher energetic neutrinos than those that have ever been detected. Moreover, it is clear how the choice of beam configuration plays a crucial role in determining the sensitivity of a telescope

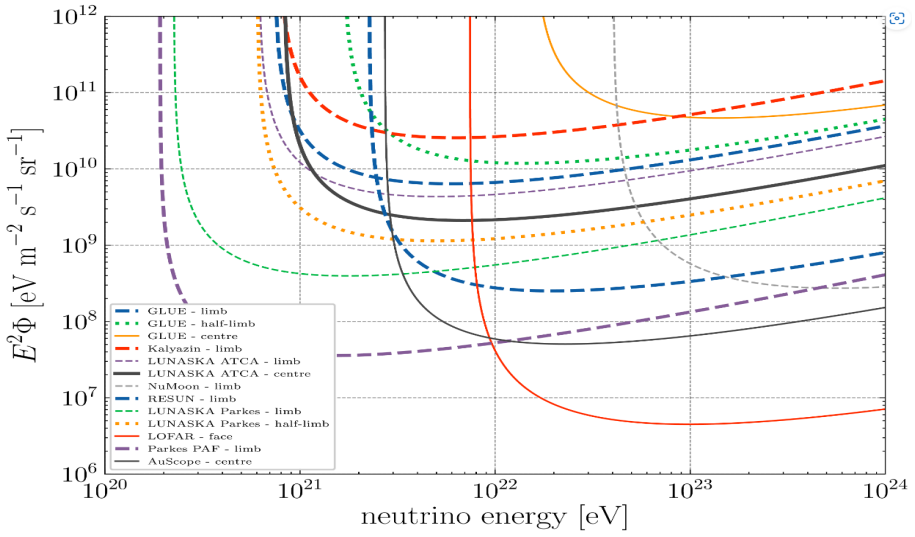

Figure 4.9: Limits on the diffuse neutrino flux set by past experiments and for comparison by some future experiments such as LOFAR, Parkes PAF and AuScope from reproducing publicly available data and using the analytic method of Gayley et al.

to lunar origin pulses. Since beam configuration is inextricably linked to the total possible collecting surface of the moon, which in turn is a measure of the detection probability, noticeable limits' deviations occur even in the same experiment as for example with GLUE (center, limb and half-limb), LUNASKA ATCA (limb, center) and LUNASKA Parkes (limb, half-limb).

With the existence of multiple experiments of different methods, of different techniques for observing the lunar pulses and consequently of different sensitivities, we have as a result the reduction of the probability of making an error in terms of the theoretically establishment of the neutrino properties or during storage and reconstruction procedures where several decisions and approximations about parameters are made. This also enables scientists to compare between different outcomes of experiments and use this feedback for designing with better accuracy the experiments to come.

4.5 Argos telescope

Argos program is a conceptual design study of three years duration with a launch year of 2023 created with the overarching objective of the subsequent rapid implementation of a next generation telescope capable of performing multi-messenger astronomy. This design program has as a deliverable the

construction of an ARGOS-pathfinder, a scaled-down prototype of the instrument, which will be assembled at the last phase of the project by the end of 2025. The phase of construction of a leading-edge astronomical instrument in terms of Europe will begin soon after. Psiloritis mountain in Crete, where the Skinakas Observatory is located at an altitude of 1750m, is the main candidate deployment site of the upcoming Argos telescope. Crete being in the southern part of the Aegean and part of the Mediterranean Sea constitutes a radio quite site suitable for the implementing radio observations.

The Argos telescope will enable a wide-field survey of the sky, thus allowing for lunar observations a field of view that covers the entire surface of the Moon, including the limbs which implies an effective limb coverage parameter ζ of 100%. Its bandwidth value is about 2GHz being sensitive to frequencies between 1 and 3 GHz. The noise of the receiver (T_{inst}) is estimated at 25K. The total collecting area is $A_{phys} = 30.000m^2$ with a total number of elements-antennas ranging between 1000 and 1200 each of diameter of 6m. The central frequency for our lunar observation experiment will be 2 GHz and the pointing configuration will be consisted of one beam centered in the middle of the moon ($n_{beams} = 1$). The effective observing time has been left as a free parameter but in our experiment with Argos is going to range from 100 to 1000 hours of observations to calculate different sensitivity limits for observing an event. Its value can change continuously in the course of the experiment with the aim of finding the minimum time needed to detect an event. The majority of the experiments under comparison (section 4.4) had corresponding observing times between 100 and 200 hours. Moreover, an analytic calculation of the minimum electric filed strength ϵ_{min} is performed in section 4.6 leading to a minimum detection threshold value of $0,0260\mu V/m/MHz$. Some of the basic characteristics of the Argos telescope are summarized in Table 1.

Following the procedure applied in Gayley et al ([35]) experiment we assume that all the detectable particle cascades occur in the regolith which has a density of $\rho = 1,8\frac{gr}{cm^3}$ and a refractive index of $n_r = 1,73$. This approximation is called "near surface emission approximation". There are though other experiments as those of James and Protheroe ([34]) that base their simulations on dividing the lunar surface to a thin layer of regolith with depth up to 10m and an underlying layer called the sub-regolith with depth up to 2000m with a different density of $\rho = 3\frac{gr}{cm^3}$ and different attenuation lengths for the neutrinos.

For the calculation of the dispersion measure of the Argos telescope we set as inputs in the relation (number) the minimum and maximum frequencies of the Argos bandwidth which are 1 and 3 GHz respectively and a typical night time (between 10 p.m. and 6 a.m.) value for the total electron column density

(or Dm) of $7 \cdot TECU = 7 \cdot 10^{12} e^- \cdot cm^{-2}$. Hourly figures for changes in the dispersion measure are provided by NASA and its Global Navigation Satellite System (GNSS). The dispersion delay between two edges of the bandwidth cannot exceed or be comparable to the length of a pulse for the components of the pulse to be completely detected (with no loss of amplitude) and stored for later processing.

The dispersion measure determines the minimum sampling rate needed to be able to detect and reconstruct a lunar pulse completely. With sampling by definition is meant a process of converting a signal (e.g. a function of continuous time) into a sequence of discrete values (a function of discrete time). Due to a finite sampling rate a pulse would not always being sampled at its peak. Substituting the values above in the relation (4.4) we calculate a pulse delay in our bandwidth of the order of $\Delta t = 8,34ns$. Therefore for our telescope to be capable of storing the whole range of the pulse without losing a fraction of its amplitude, the minimum sampling rate per second should be

$$\frac{1s}{8,34 \cdot 10^{-9} s} = 0,12 \frac{Gsamples}{s} \tag{4.10}$$

Argos telescope will also be equiped with state-of-the-art subsystems (front-end, back-end, software). More specifically will provide optimized digital signal processing software, artificial intelligence (AI)-based image reconstruction algorithms, high resolution of the order of 5 arcsec, detection in real-time, will be able of simultaneous recording of two orthogonal polarizations since being equipped with dual linear polarization and to handle a large amount of data either for processing or output. All its results will be made publicly available. These aforementioned capabilities are expected to have a major scientific impact. Its primary objective of optimal integration into the network of existing and future international astronomical infrastructures will maximize its long-term impact.

Experiment	pointing	$\nu(MHz)$	$\Delta\nu(MHz)$	$\zeta(100\%)$	$\epsilon_{min}(\mu V/m/MHz)$	$t_{obs}(h)$
Argos	centre	2000	2000	100	0,0260	100-1000

Table 4.1: Observations parameters for the Argos lunar radio experiment

4.6 Neutrino flux limits with Argos telescope

The ultimate target of this section is to provide results for the sensitivity limits of the Argos telescope to neutrino fluxes and be compared to observational and simulated data. To achieve this goal an independent way to calculate the limits based on the work of Gayley et al ([35]) is followed. The following results could be considered as a good comparison factor between conducted lunar experiments but not as a completely accurate measure of their absolute sensitivity to neutrinos. Further future development of models calculating analytically the effective aperture and sensitivity to neutrino fluxes is strongly motivated.

Gayley et al ([35])used an analytic way to describe the sensitivity of the effective aperture of the lunar regolith to UHE neutrino fluxes rather than the commonly used simulations from previous works of their predecessors (reference). They concluded to an analytic expression for the effective aperture defining also analytic expressions for each individual parameter that inserts their analytic formula. In order to obtain a result in a closed form they had to make several approximations such as constant elasticity for neutrino-nucleon interactions ($E_s = 0, 2E_v$), a fixed limb coverage parameter, a constant transmission coefficient and no losses for radiation passing through the boundary of the regolith to reach space ($t_{\|} = 0, 6$), a "near surface emission approximation" as described above, a "small angle approximation" (assuming that a particle can be detectable only from a point very close to the Cherenkov angle) and assuming no effects from small-scale surface roughness.

Having access to closed-form expressions is kind of revolutionary as there are not such expressions currently available in the literature. This procedure is much more convenient in terms of calculating the effective aperture but can also yield the means for optimizing the experimental design assisting in penetrating deeper into the recesses of the uncharted neutrino region.

4.6.1 Flux limit formula

The flux of neutrino particles can be defined as:

$$F_{neutrino} = \frac{d^3N}{dAdtd\Omega} \tag{4.11}$$

and in order to express the flux as a function of energy the differential ratio

$$\frac{dF_{neutrino}}{dE} = \frac{d^3N}{dAdtd\Omega} \tag{4.12}$$

is necessary. The most commonly plotted quantity in neutrino fluxes experiments is the

$$F_{energy,v}(E) = E^2 \Phi_{iso,\nu}(E) \tag{4.13}$$

measured in $\frac{eV}{m^2 \cdot sr \cdot s}$ where $\Phi_{iso,\nu}(E)$ stands for the differential neutrino flux $\frac{dF_{neutrino}(E)}{dE}$. With current interest in high-energy particle experiments being mainly reflected in cosmologically distributed sources, rather than specifically targeted sources, measurements of the neutrino fluxes focus on isotropic neutrino flux distributions $\Phi_\nu(E)$ in order to cover larger regions of the visible universe.

High energy physicists traditionally report errors on results of experiments based on the classical confidence intervals. A classical confidence interval (CI) is a range of estimates for an unknown parameter (e.g. the neutrino detection events) and is computed at a designated confidence level. More specifically, it is the interval between which a true value for a parameter measured is expected to lie at the given confidence level. The larger the sample available, the narrowest the confidence interval would be.

The ANITA-III ([30]) 90% confidence level limit on the all-flavor-sum diffuse neutrino flux is set by using:

$$\frac{Ed^4N}{dEdAd\Omega dt} = \frac{s_{upp}}{T\epsilon_{ana}(E_\nu) < A\Omega > (E)\Delta} \tag{4.14}$$

where s_{upper} is the upper side of the confidence interval for a 90% confidence level and Δ is a parameter corresponding to the bin-width. Bin-width is transformed into log space for convenience. The parameter ϵ_{ana} is an efficiency factor about the analysis method followed for ANITA-III experiment ([30]) and is not taken into account for our calculation. Due to dimensional equality between the two sides the factor Δ is dimensionless corresponding to the ratio $\frac{dE}{E}$, hence its designation as bin-width. Using the derivative of lnE:

$$\frac{dln(E)}{dE} = \frac{1}{E} \tag{4.15}$$

and a change in the base of the logarithm ($dlnE = ln(10)dlogE$) it holds that:

$$\Delta = ln(10)dlogE \tag{4.16}$$

To obtain the desired plotted quantity we multiply equation (number) with E and conclude to:

$$\frac{E^2d^4N}{dEdAd\Omega dt} = \frac{s_{upp}E}{T\ < A\Omega > (E)\Delta} \tag{4.17}$$

In Bray's paper ([33]) the 90% CL limit to a diffuse isotropic neutrino flux, assuming zero detected events, is given by:

$$\frac{dF_{iso}}{dE} < 2,3\frac{1}{EX(E)} \tag{4.18}$$

where $X(E)$ expresses the total exposure to neutrino fluxes having dimensions of area times solid angle and is given by the relation:

$$X(E) = \sum_{P} A_P(E) t_{obs,P} \tag{4.19}$$

Each individual pointing configuration P corresponds to a different effective aperture $A_P(E)$ which is calculated separately. In our experiment though there is only one beam and one pointing configuration targeting the entire moon. Therefore the analytic calculation of the effective aperture will be performed once. Multiplying both sides of equation (4.18) with the positive quantity E^2 lead to the following:

$$F(E) < 2,3\frac{E}{t_{obs}A(E)} \tag{4.20}$$

which is the relation (68) of Gayley et al. ([35]). In both the last two relations for the diffuse isotropic neutrino fluxes the factor Δ is considered to be unity so the term $d\log E$ is assumed to be equal to $\frac{1}{\ln 10}$. Thus for our Argos experiment assuming the same value of Δ and zero detected events for the time we observe, the 90% CL limit to a diffuse isotropic neutrino flux is given by the formula:

$$\frac{E^2 dF_{iso}}{dE} = 2,44E\frac{1}{t_{obs}A(E)} \tag{4.21}$$

where the upper limit of the confidence interval was chosen from Table IV of Feldman and Cousins ([36]) regarding a Poisson distribution for a signal mean. For zero detected events, that is, zero observed events and zero background events, the confidence interval with 90% confidence level is between the values of zero and 2,44. The value of 2,44 is interpreted as the maximum true events that may have existed and gone undetected. For true events with a value over 2,44 we expect a detected event. It should be noted that the 90% confidence level leaves a margin for a 10% chance that there may have existed more than 2,44 events that were not detected. Thus 2,44 is the lowest limit of true events for which the detector can capture one event. In other words, for moon produced events less than 2,44, our telescope will not be able to detect any event.

4.6.2 Effective aperture and minimum threshold

For the analytic calculation of the effective aperture we follow the procedure described in Gayley et al paper ([35]) or as it is summarized in the Appendix B in Bray's paper ([33]). The analytic formula for the effective aperture as a function of the initial incident neutrino energy is given by:

$$A_v(E) = A_0 \cdot \zeta \cdot \frac{n_r^2 - 1}{8n_r} \cdot \frac{L_\gamma}{L_\nu} \cdot f_0^3 \cdot \Delta_0 \cdot (\psi_{ds} + \psi_{dr} + \psi_u) \tag{4.22}$$

where the limb coverage dependence ζ has been inserted inside the relation. The parameter ζ, since representing the fraction of the circumference observed, acts as a scaling of the results and in our experiment corresponds to maximum scale ($\zeta = 100\%$). The refractive index has a constant value $n_r = 1,73$ and A_0 represents the maximum possible aperture to an isotropic flux of neutrinos assuming that the moon was a perfect detector:

$$A_0 = 4\pi R^2 \tag{4.23}$$

where R is the radius of the moon with a value of $R = 1,738 \cdot 10^6 m$.

Moreover the parameters L_γ and L_ν represent the electric field dissipation length or the photon mean free path and the neutrino attenuation length in the lunar regolith respectively and are given by the analytic formulae of Gayley et al ([35]):

$$L_\gamma = 5 \cdot 10^{-6} R(\frac{v}{GHz})^{-1} \tag{4.24}$$

which is a function of the central frequency v and

$$L_\nu = 7 \cdot 10^{-2} R(\frac{E_v}{10^{20} eV})^{-\frac{1}{3}} \tag{4.25}$$

which is a function of the neutrino energy. Δ_0 parameter characterizes the width of the Cherenkov cone with the angle (1/e half width) whereas f_0 is a dimensionless parameter that describes how far the receiver can be from the Cherenkov cone while observing an electric field above the threshold ϵ_{min}. The Δ_0 parameter is given by the analytic formula:

$$\Delta_0 = 0,05(\frac{\nu}{GHz})^{-1}\big\{1 + 0,075 log(\frac{E_S}{10^{19} eV})\big\}^{-1} \tag{4.26}$$

which is a function of the shower energy.

In our calculation as also in that of Gayley et al ([35]) or Bray ([33]), to the hadronic particle shower energy E_s is attributed only the 20% of the incident energy of the primary neutrino, that is

$$E_S = 0,2 E_\nu \tag{4.27}$$

On the other hand the dimensionless parameter f_0 can either be estimated by the ratio of $\frac{\Delta_C}{\Delta_0}$ where Δ_C is the Cherenkov width with the angle at ϵ_{min} or by the analytic formula:

$$f_0 = \sqrt{ln(\frac{\epsilon_0 \cdot t_{\parallel}}{\epsilon_{min}})} \tag{4.28}$$

The transmission coefficient has a constant value given by the Table 1 whereas the ϵ_0 variable corresponds to the peak of the electric field and is calculated by the analytic expression:

$$\epsilon_0 = 0,0845\frac{\nu}{m \cdot MHz}(\frac{d}{m})^{-1}(\frac{E_S}{10^{18}eV})(\frac{\nu}{GHz})\{1+(\frac{\nu}{2,32GHz})^{1,23}\}^{-1} \tag{4.29}$$

In addition the parameter σ_0 represents the root mean square (rms) surface roughness angle which with the multiplication of the $\sqrt{2}$ factor is converted to the 1/e half width of a Gaussian distribution of unidirectional surface slopes. Its formula is given by:

$$\sigma_0 = \sqrt{2}tan^{-1}\big(0,14(\frac{\nu}{GHz})^{0,22}\big) \tag{4.30}$$

and is measured in radians.

For the calculation of ϵ_{min} given by the relation (number) first calculating the parameters T_{sys}, A_{eff}, f_C, n_σ, $B(\theta)$, η and α whose physical meaning has been discussed in detail in section 4.3 is inevitable. The system temperature is given by the formula:

$$T_{sys} = T_{inst} + T_{moon} \tag{4.31}$$

which corresponds to with $T_{inst} = 25K$ for our Argos telescope and $T_{moon} = 225K$ due to blackbody thermal emission from the Moon. It is because of our beam forming consisted of a single beam pointing at the center of the Moon that we do not take into account contribution from Galactic Synchrotron emission. A_{eff} is estimated by the product of total collecting area $A_{phys} = 30.000m^2$ and the Argos aperture efficiency $e_\alpha = 0,8$ resulting in $A_{eff} = 24.000km^2$. In Argos experiment we combine signals from multiple channels, 65536 in number, for the detection of a radio pulse. To estimate the sensitivity of combining different channels we should take into account that sensitivity is highly dependent on whether there is phase coherence between the channels and whether they are combined coherently. Combining coherently implies the direct summation of the signals' voltages while incoherently combination implies the summation of the squared voltages. In Argos the

combination of the channels is done coherently, that is, the channels act as a single channel. In this case the scaling of the minimum threshold is proportional to $f_C = C^{-\frac{1}{2}} = \sqrt{\frac{1}{65536}} = \frac{1}{256}$.

Furthermore in Argos using dual linear polarization we know the angle at which the incoming signal is incident to our receiver. For a random event we need to calculate an average of the incident angle. Therefore assuming parallel rays from the Moon due to the small distance from Earth, that is assuming θ fixed, we calculate a 2D integral for the quantity $\frac{1}{cos^2\phi}$ which gives a factor of $\frac{1}{2}$ as a result which corresponds to $\eta = 2$. Determining the position angle of the linear polarization ϕ gives the position around the Cherenkov cone centered on the event. An interferometer like Argos can measure the location of the event on the moon, and can give as a result the position of the UHE neutrino source on the sky.

The complete recovery of the signal's initial amplitude expressed through the α parameter (described analytically in section 4.3) can be achieved for our Argos telescope due to exclusion of inefficiencies during reconstruction of the pulse. Specifically, using dual polarization in our receivers, through the measurement of the fraction of amplitude in each polarization and the use of simple geometry, we can avoid any losses. In addition using efficient sampling rate of the order of $0,12\cdot$ Gsamples/s we can achieve storage of all the components of the dispersed pulse for our bandwidth and recover the true value of the initial pulse's amplitude. With Argos being capable of achieving these requirements we set as value of α the unit assuming no amplitude loss.

As mentioned in section 4.3 the parameter n_σ expresses a significance threshold for exclusion of unwanted events whose presence overloads our data storage capability and increase the time needed for post-analysis. Taking as a threshold initial value for triggering the value of 5σ we can as a first step to store the efficient data for a post-analysis. Later after having results from the analysis, after having measured the signal to noise ratio from our stored data and having excluded RFI events via the use of off-line cuts we are going to derive the maximum excluded threshold for an event which in the next moment is going to become our minimum significance threshold for exclusion. In our calculation we have set as input for the n_σ parameter the value 10σ which is a common value for many lunar experiments close to Argos basic characteristics such as SKA.

Assuming a radially symmetric beam power $B(\theta)$ the surface of our telescope can be approximated by an Airy disk. The intensity of light of an Airy disk is given by the formula:

$$I(\theta) = I(0) \cdot \big(\frac{2J_1(k\alpha \sin(\theta))}{ka \sin(\theta)}\big)^2 \tag{4.32}$$

where $I(0)$ is the normalization for a beam intensity in the central axis, k is the wavenumber, α is the effective radius of the telescope, J_1 is the Bessel function of the first kind of the order one and θ is the angle through which our telescope observes the total lunar surface. The relation for the beam intensity can be integrated to extract the total power $B(\theta)$ contained in an Airy disk of a given size. Since the Moon moves in a nearly circular elliptical orbit around the Earth, the distance between the Earth and the Moon is a varying quantity, ranging from $363,2km$ up to $405,4km$, that results in variability in the apparent size of the moon as well whose values range between 29' and 34'. This variability depends on the coordinates of our telescope as well as its altitude. Provided that the Moon covers approximately half a degree on the celestial sphere in one hour, we cannot be sure of the exact apparent size of the Moon that corresponds to each of our measurements during a nighttime observation. Applying the range of values for the apparent size to the intensity formula and integrated it, from the analysis of the results we take as a typical value for the beam power $B(\theta) = 0,04W$.

Having calculated all the parameters on which the minimum threshold depends on, we conclude to the nominal value of $\epsilon_{min} = 0,0260\mu V/m/Hz$.

Finally the terms in the parentheses account for the presence or not of the surface roughness effects. The ψ_{ds} term accounts for downward neutrinos interacting with a smooth moon surface whereas the ψ_{dr} term accounts for downward detections of neutrinos assisted by the presence of surface roughness. Both parameters are calculated through parameters introduced above and their values are calculated by the expressions:

$$\psi_{ds} = f_0 \cdot \Delta_0 \tag{4.33}$$

and

$$\psi_{dr} = 0,96a_0 \tag{4.34}$$

respectively. Last but not least the parameter ψ_u accounts for upwards neutrinos that have penetrated the surface without being attenuated in their descent and is found through the expression:

$$\psi_u = 5,3a_0 \tag{4.35}$$

where a_0 represents the maximum angle with respect to the lunar surface for which a neutrino penetrates the Lunar regolith without being attenuated. For a_0 we use the formula:

$$a_0 = 0,03(\frac{E}{10^{20}eV})^{-\frac{1}{3}} \tag{4.36}$$

Whichever of these three terms of the parentheses is largest, dominates the effective neutrino aperture. Roughness is an important contributor to the aperture as for high frequencies over 1GHz, which coincide with the detection frequency range of our Argos telescope, σ_0 (ψ_{dr}) has a large scale over 10 degrees whereas on the other hand for low frequencies the ψ_{ds} term dominates. In lunar radio experiments where the detection frequencies are high, the Earth-like distances and our telescope's apertures (collecting areas) are comparatively small, lunar surface roughness is a crucial parameter that should not be omitted.

4.6.3 Results with Argos / Discussion

Having defined all the necessary parameters for the analytic formula of the effective aperture all that remains is to determine the effective observation time for our Argos experiment. For t_{obs} corresponding to 100, 200, 500 and 1000h of observations we plot the sensitivity of the Argos telescope to neutrino fluxes, combining equations (4.21) and (4.22), compared to the limits of past and future experiments already mentioned in section 4.6.

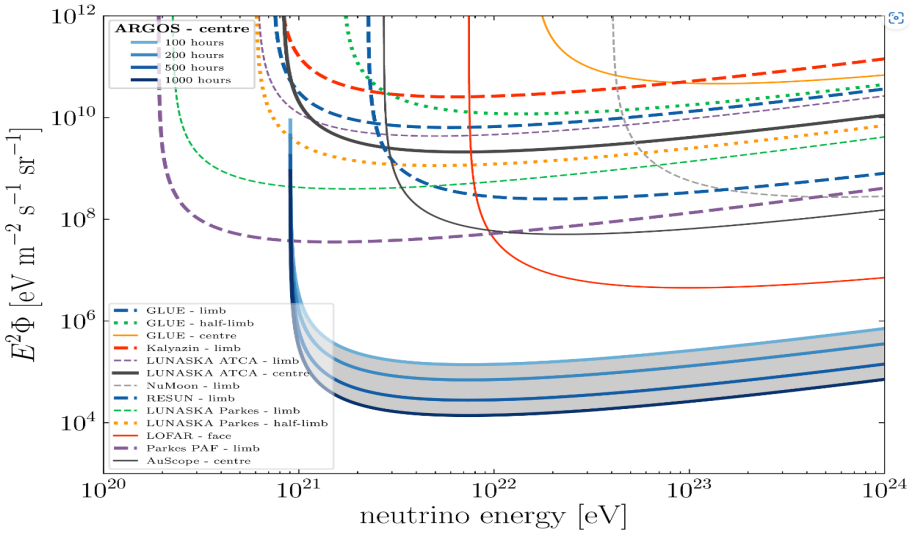

Figure 4.10: Limits on the diffuse neutrino flux with Argos telescope using the analytic calculation described in this section compared to past experiments such as GLUE, Kalyazin, LUNASKA, RESUN, NuMoon and future experiments such as LOFAR, Parkes PAF and AuScope. Limits are shown for different values of observing time (blue and light blue solid lines).

The results of our calculation show that our Argos telescope is sensitive to neutrino energies from $10^{21}eV$ and above. These sensitivity limits are

comparable to those to which many experiments are sensitive to such as LUNASKA ATCA having a beam configuration pointing at the center but also as RESUN limb, Kalyazin limb, LUNASKA ATCA limb and LUNASKA Parkes limb. Argos telescope seems to be more sensitive to higher energy neutrinos, and thus less sensitive to the expected values of neutrinos close to the GZK cut-off around $10^{19,6}eV$ and below, than the future experiment Parkes PAF (more right in the diagram). At the same time Argos is less sensitive to higher energy neutrinos, meaning more sensitive to cosmogenic neutrinos, than future experiments as AuScope with centre pointing configuration and LOFAR with face configuration. Moreover it is clear that the plotted quantity $E^2\Phi_\nu$ is dependent on the observation hours with the Argos thus being more capable of detecting lower neutrino fluxes as the hours of observations are increased.This translates into fewer actual events being required to detect an event compared to fewer observation hours meaning greater sensitivity to neutrinos.

Argos telescope sensitivity as being sensitive to neutrino energies over the GZK cut-off and over the most energetic neutrino event ever observed (around $3 \cdot 10^{20}eV$) implies that a positive detection of a neutrino event could serve as an important statement supporting the theory of existence of exotic sources capable of producing even higher energies than the conventional acceleration scenarios ever predicted. All that remains as a next step is to build our Argos telescope and wait patiently for some detectable events that will signal the entry into the fields of the new high energy -particle physics.

Chapter 5

Conclusion

Having embarked on the journey of finding answers to the most profound questions of high energy particle physics and cosmology such as that of finding the UHE cosmic ray sources that may take us back to the beginnings of the universe, we witnessed how particles like neutrinos having almost zero mass and charge, being weakly or not at all interacting with the bulk of the cosmic matter may hold within them the greatest information for solving a significant part of the never-ending puzzle of cosmological physics. High-energy neutrinos, these elusive particles, are proving in practice to be the most prominent and valuable particles to study. Countless attempts made, endless hours of human work spent in neutrino physics to possibly detect a few, maybe one or even zero events over a whole year.

Argos strongly declares its involvement in the effort to study and understand UHE cosmogenic neutrinos with the upcoming construction of the next-generation telescope that will aim to detect them through the neighboring Moon surface. The detection or not of neutrinos with the Argos, one way or another, will unlock the path of the labyrinth that encloses the secrets of our cosmic sources taking us on an interesting journey back in time.

Completing this study the conclusion we can draw with absolute certainty is that without understanding neutrinos we will never be able to fully understand the universe.

Bibliography

[1] Bhattacharjee, P., Sigl, G. (2000). Origin and propagation of extremely high-energy cosmic rays. Physics Reports, 327(3-4), 109-247.

[2] Torres, D. F., Anchordoqui, L. A. (2004). Astrophysical origins of ultra-high energy cosmic rays. Reports on Progress in Physics, 67(9), 1663

[3] Bhattacharjee, P., Hill, C. T., Schramm, D. N. (1992). Grand unified theories, topological defects, and ultrahigh-energy cosmic rays. Physical Review Letters, 69(4), 567.

[4] Blasi, P. (2013). The origin of galactic cosmic rays. The Astronomy and Astrophysics Review, 21, 1-73

[5] Greisen, K. (1966). End to the cosmic-ray spectrum?. Physical Review Letters, 16(17), 748.

[6] Beresinsky, V. S., Zatsepin, G. T. (1969). Cosmic rays at ultra high energies (neutrino?). Physics Letters B, 28(6), 423-424.

[7] Ptuskin, V. (2012). Propagation of galactic cosmic rays. Astroparticle Physics, 39, 44-51

[8] Allard, D., Parizot, E., Olinto, A. V. (2007). On the transition from galactic to extragalactic cosmic-rays: Spectral and composition features from two opposite scenarios. Astroparticle Physics, 27(1), 61-75.

[9] Allard, D. (2012). Extragalactic propagation of ultrahigh energy cosmic-rays. Astroparticle Physics, 39, 33-43.

[10] Allard, D., Parizot, E., Olinto, A. V., Khan, E., Goriely, S. (2005). UHE nuclei propagation and the interpretation of the ankle in the cosmic-ray spectrum. Astronomy and Astrophysics, 443(3), L29-L32.

[11] Allard, D., Decerprit, G., Olinto, A. V., Parizot, E. (2008). Implications of the cosmic ray spectrum for the mass composition at the highest energies. Journal of Cosmology and Astroparticle Physics, 2008(10), 033.

[12] Aloisio, R., Berezinsky, V., Blasi, P. (2014). Ultra high energy cosmic rays: implications of Auger data for source spectra and chemical composition. Journal of Cosmology and Astroparticle Physics, 2014(10), 020.

[13] Abraham, J., Abreu, P., Aglietta, M., Aguirre, C., Allard, D., Allekotte, I., ... Gonçalves, P. (2007). Correlation of the highest-energy cosmic rays with nearby extragalactic objects. Science, 318(5852), 938-943.

[14] Allard, D., Olinto, A., Ave, M., Parizot, E. (2008). Cosmogenic Neutrinos from the propagation of Ultra High Energy Cosmic Rays. In International Cosmic Ray Conference (Vol. 3, pp. 1249-1252).

[15] Allard, D. (2009). Cosmogenic neutrino production from the propagation of ultra-high energy cosmic-ray nuclei. Nuclear Physics B-Proceedings Supplements, 188, 293-295.

[16] Aloisio, R., Boncioli, D., Di Matteo, A., Grillo, A. F., Petrera, S., Salamida, F. (2015). Cosmogenic neutrinos and ultra-high energy cosmic ray models. Journal of Cosmology and Astroparticle Physics, 2015(10), 006.

[17] Kotera, K., Allard, D., Olinto, A. V. (2010). Cosmogenic neutrinos: parameter space and detectabilty from PeV to ZeV. Journal of Cosmology and Astroparticle Physics, 2010(10), 013.

[18] Engel, R., Seckel, D., Stanev, T. (2001). Neutrinos from propagation of ultrahigh energy protons. Physical Review D, 64(9), 093010.

[19] Stanev, T., De Marco, D., Malkan, M. A., Stecker, F. W. (2006). Cosmogenic neutrinos from cosmic ray interactions with extragalactic infrared photons. Physical Review D, 73(4), 043003.

[20] Stanev, T. (2006). Ultra high energy neutrinos: the key to ultra high energy cosmic rays. arXiv preprint astro-ph/0607515.

[21] Aloisio, R., Boncioli, D., di Matteo, A., Grillo, A. F., Petrera, S., Salamida, F. (2015). SimProp v2r2: a Monte Carlo simulation to compute cosmogenic neutrino fluxes. arXiv preprint arXiv:1505.01347.

[22] Schröder, F. G. (2017). Radio detection of cosmic-ray air showers and high-energy neutrinos. Progress in Particle and Nuclear Physics, 93, 1-68.

[23] Ekers, R. D., James, C. W., Protheroe, R. J., McFadden, R. A. (2009). Lunar radio Cherenkov observations of UHE neutrinos. Nuclear Instruments and Methods in Physics Research Section A: Accelerators, Spectrometers, Detectors and Associated Equipment, 604(1-2), S106-S111.

[24] Bray, J. D., Ekers, R. D., Roberts, P., Reynolds, J. E., James, C. W., Phillips, C. J., ... Alvarez-Muñiz, J. (2012). Status and strategies of current LUNASKA lunar Cherenkov observations with the Parkes radio telescope. Nuclear Instruments and Methods in Physics Research Section A: Accelerators, Spectrometers, Detectors and Associated Equipment, 662, S95-S98.

[25] James, C. W., Ekers, R. D., Alvarez-Muniz, J., Protheroe, R. J., McFadden, R. A., Phillips, C. J., Roberts, P. (2009). Status report and future prospects on LUNASKA lunar observations with ATCA. Nuclear Instruments and Methods in Physics Research Section A: Accelerators, Spectrometers, Detectors and Associated Equipment, 604(1-2), S112-S115.

[26] Bray, J. D., Alvarez-Muniz, J., Buitink, S., Dagkesamanskii, R. D., Ekers, R. D., Falcke, H., ... ter Veen, S. (2014). Lunar detection of ultra-high-energy cosmic rays and neutrinos with the Square Kilometre Array. arXiv preprint arXiv:1408.6069.

[27] James, C. W., Alvarez-Muniz, J., Bray, J. D., Buitink, S., Dagkesamanskii, R. D., Ekers, R. D., ... ter Veen, S. (2016). The lunar askaryan technique with the square kilometre array. arXiv preprint arXiv:1608.02408.

[28] James, C. W., Bray, J. D., Ekers, R. D. (2019). Prospects for detecting ultra-high-energy particles with FAST. Research in Astronomy and Astrophysics, 19(2), 019.

[29] Gorham, P. W., Hebert, C. L., Liewer, K. M., Naudet, C. J., Saltzberg, D., Williams, D. (2004). Experimental limit on the cosmic diffuse ultrahigh energy neutrino flux. Physical Review Letters, 93(4), 041101.

[30] Gorham, P. W., Allison, P., Banerjee, O., Batten, L., Beatty, J. J., Bechtol, K., ... Anita Collaboration. (2018). Constraints on the diffuse high-energy neutrino flux from the third flight of ANITA. Physical Review D, 98(2), 022001.

[31] James, C. W., Crocker, R. M., Ekers, R. D., Hankins, T. H., O'Sullivan, J. D., Protheroe, R. J. (2007). Limit on ultrahigh energy neutrino flux from the Parkes Lunar Radio Cherenkov experiment. Monthly Notices of the Royal Astronomical Society, 379(3), 1037-1041.

[32] Kravchenko, I., Cooley, C., Hussain, S., Seckel, D., Wahrlich, P., Adams, J., ... Ratzlaff, K. (2006). Rice limits on the diffuse ultrahigh energy neutrino flux. Physical Review D, 73(8), 082002.

[33] Bray, J. D. (2016). The sensitivity of past and near-future lunar radio experiments to ultra-high-energy cosmic rays and neutrinos. Astroparticle Physics, 77, 1-20.

[34] James, C. W., Protheroe, R. J. (2009). The sensitivity of the next generation of lunar Cherenkov observations to UHE neutrinos and cosmic rays. Astroparticle Physics, 30(6), 318-332.

[35] Gayley, K. G., Mutel, R. L., Jaeger, T. R. (2009). Analytic aperture calculation and scaling laws for radio detection of lunar-target ultra-high-energy neutrinos. The Astrophysical Journal, 706(2), 1556.

[36] Feldman, G. J., Cousins, R. D. (1998). Unified approach to the classical statistical analysis of small signals. Physical review D, 57(7), 3873.